Immunosuppression broadens evolutionary pathways to treatment failure during *Acinetobacter baumannii* pneumonia

Wenwen Huo[1,§], Lindsay M. Busch [1,2,§], Juan Hernandez-Bird[1], Efrat Hamami[1], Christopher W. Marshall[3,4], Edward Geisinger[5], Vaughn S. Cooper[3], Tim van Opijnen[6], Jason W. Rosch[7] and Ralph R. Isberg[1,*]

[1]Department of Molecular Biology and Microbiology, Tufts University School of Medicine, 150 Harrison Ave., Boston, MA 02111, USA.

[2]Current address: Division of Infectious Diseases, Emory University School of Medicine

[3]Department of Microbiology and Molecular Genetics and Center for Evolutionary Biology and Medicine, University of Pittsburgh School of Medicine, Pittsburgh, Pennsylvania, USA.

[4]Current Address: Dept. of Biological Sciences, Marquette University, 1428 W. Clybourn St., Milwaukee, WI. 53233.

[5]Department of Biology, Northeastern University, Boston, MA, 02115, USA

28 [6]Department of Biology, Boston College, Boston, MA, USA.

29

30 [7]Department of Infectious Diseases, St Jude Children's Research Hospital, Memphis, TN, USA.

31

32 [§]Equal contributions.

33 [*]Corresponding Author

Abstract

Acinetobacter baumannii is increasingly refractory to antibiotic treatment in healthcare settings. As is true of most human pathogens, the genetic path to antimicrobial resistance (AMR) and the role that the immune system plays in modulating AMR during disease are poorly understood. Here we reproduced several routes to fluoroquinolone resistance, performing evolution experiments using sequential lung infections in mice that are replete or depleted of neutrophils, providing two key insights into the evolution of drug resistance. First, neutropenic hosts acted as reservoirs for the accumulation of drug resistance during drug treatment. Selection for variants with altered drug sensitivity profiles arose readily in the absence of neutrophils, while immunocompetent animals restricted the appearance of these variants. Secondly, antibiotic treatment failure in the immunocompromised host was shown to occur without clinically defined resistance, an unexpected result that provides a model for how antibiotic failure occurs clinically in the absence of AMR. The genetic mechanism underlying both these results is initiated by mutations activating the drug egress pump regulator AdeL, which drives persistence in the presence of antibiotic. Therefore, antibiotic persistence mutations present a two-pronged risk during disease, causing drug treatment failure in the immunocompromised host while simultaneously increasing the emergence of high-level AMR.

52 # Introduction

53 *Acinetobacter baumannii* is a Gram-negative opportunistic pathogen, one of the high-
54 priority ESKAPE organisms that are increasingly difficult to treat due to multiple antibiotic
55 resistance[1]. A significant proportion of healthcare-associated diseases caused by this group of
56 pathogens, such as ventilator associated pneumonia, is linked to their documented multi-drug
57 resistance (MDR) [2-5]. Of particular importance are patients in intensive care units (ICU) who are
58 critically ill and have depressed immunological clearance mechanisms that increase the risk of
59 infection by MDR pathogens [6,7]. As a consequence, the healthcare environment with its
60 immunologically compromised patients could provide a unique niche for selection of MDR isolates
61 [8]. Overlaying these issues is the fact that for many patients in healthcare settings, antibiotic
62 treatment failure is common but is often unexplained, as resistant organisms cannot be identified[9].

63 *A. baumannii* clinical isolates have demonstrated a remarkable ability to successfully battle
64 antibiotic treatment in the clinic, resulting from high intrinsic resistance to antimicrobials and the
65 acquisition of drug resistance elements by the organism[10,11,12, 13]. A critical missing link is a detailed
66 roadmap for the stepwise evolution of antibiotic resistance in the clinic, particularly in identifying
67 *A. baumannii* subpopulations most likely to give rise to drug treatment failure. Furthermore, it is
68 largely unknown if there exists a patient group that provides the reservoir for antimicrobial
69 resistance (AMR) acquisition. Particularly for healthcare-associated diseases, patient groups
70 susceptible to *A. baumannii* are by their nature compromised in a number of fashions, with the
71 potential for providing reservoirs for AMR evolution. The range of individuals with altered immune
72 function in these settings may allow for a diversity of host targets that can act as primary amplifiers
73 of resistance, with eventual spread to individuals with different sets of susceptibilities. Therefore,
74 as a model for healthcare-associated pneumonia we aimed to explore whether depletion of a single

75 arm of innate immunity in mice could help shape the antibiotic treatment outcome and support the
76 evolution of resistant organisms.

77 Fluoroquinolones (FQ) such as ciprofloxacin initially showed excellent activity against *A.*
78 *baumannii* infections[14]. Members of this drug class inhibit bacterial cell growth by covalently
79 linking to DNA gyrase (*gyrA*) and topoisomerase IV (*parC*), leading to double stranded DNA breaks
80 and cell death[15]. Drug resistant mutants arise fairly frequently in the clinic, with over 80% of
81 clinical isolates of *A. baumannii* currently being FQ resistant[16]. The most commonly reported
82 mechanisms of ciprofloxacin resistance in the clinic are target protein alterations and the
83 overexpression of efflux pumps. In *A. baumannii*, alterations in target proteins usually evolve in a
84 stepwise fashion, starting with *gyrA* (usually Ser81Leu) followed by *parC* (Ser83Leu). Interestingly,
85 in addition to the patient's underlying condition and hospitalization status, prior exposure to
86 fluoroquinolones is also a risk factor for *A. baumannii* colonization and infection[17], indicating that
87 resistance to this antibiotic class is linked to either increased pathogenic potential of the isolate or
88 is highly associated with acquisition of MDR. Unknown is whether there exist early adaptive
89 mutations that enable precursor populations of *A. baumannii* to act as ancestors to drug resistance.

90 There has been little study of whether AMR can be suppressed by the immune response.
91 Landmark mathematical modeling work argues that the immune response can largely limit the
92 outgrowth of persisters or other bacterial variants that exhibit intermediate resistance levels [18].
93 Another study indicates that the cytokine response may control waves of AMR variants[19]. Given the
94 limited analysis of how antibiotic resistance evolves in the clinic, and the lack of a detailed
95 interrogation of the role played by the immune response in controlling selection of AMR, we sought
96 to identify the steps that lead to resistance in the presence or absence of a single arm of innate
97 immunity. The rationale behind this approach is that clinical antibiotic resistance is associated
98 with mutations located outside well-characterized drug targets, and these are difficult to identify

99 bioinformatically or predict based on culture studies [20-22]. This approach provides evidence that
100 absence of neutrophil function allows outgrowth of drug persisters and the appearance of
101 fluoroquinolone resistance. In so doing, we identified mutational pathways to drug resistance, with
102 the results tied to the problem of unexplained antibiotic treatment failure.

103

104 # Results

105 **Recapitulation of *Acinetobacter baumannii* evolved drug resistance during pneumonic**
106 **disease.** We serially passaged *A. baumannii* 15 times within a mouse pneumonia model to analyze
107 the dynamics and genetic trajectories of resistance to the FQ antibiotic ciprofloxacin (CIP), with the
108 purpose of determining whether neutrophils play a role in suppressing drug resistance (Fig. 1A).
109 The CIP^S ATCC reference strain 17978 (AB17978) was passaged by oropharyngeal inoculation in
110 either immunocompetent animals or those depleted of neutrophils by pretreatment with two doses
111 of cyclophosphamide. It should be noted that this treatment also has other effects on the immune
112 system, including the possible reduction of monocyte populations, as well as suppressing T-cell
113 numbers [23,24]. Mice in three parallel lineages were CIP treated at 7- and 19- hours post infection
114 (hpi) and bacteria were collected from the lungs of animals euthanized at 27 hpi. The enriched
115 bacterial pools from each independent infection were used as inocula for the next round of
116 infection. The dynamics of bacterial yield was assessed from lung homogenates, and the CIP
117 minimum inhibitory concentration (MIC) of each population was determined followed by whole
118 genome sequencing of the heterogenous pool (mean genome coverage depth: 368.4).

119 **Persistent neutropenia during successive passages quickly results in antibiotic**
120 **treatment failure.** A striking result from the passage experiments is that the protocol allowed drug
121 resistant mutants to overgrow during passage in neutrophil-depleted animals, while the resistant

122 variants in the immunocompetent animal failed to reach high abundance in the population. After
123 each mouse passage in the presence of CIP, the efficiency of bacterial colonization of the lungs was
124 monitored by quantifying total bacterial colony forming units in the absence of drug (CFU).
125 Bacterial lung yields increased by 1000-fold in CIP-treated neutrophil-depleted mice over the
126 course of 15 passages, as compared to little increase in immunocompetent mice (Fig. 1B). After
127 each passage, we observed 10-fold higher colonization in the neutrophil-depleted compared to
128 immunocompetent mice. By passages 5-7, the lung bacterial load in the neutrophil-depleted mice
129 reached the size of the initial inoculum (10^8 CFU), and animals showed significant signs of disease
130 such as lacrimation, piloerection, and decreased mobility in spite of being CIP treated (Fig. 1B).

131 To determine levels of CIP resistance after each passage, the saved bacteria were quantified
132 on solid medium in the absence or presence of increasing amounts of drug, plotting the fraction of
133 surviving CFU as a function of CIP concentration (Material and Methods; Fig. 2A and 2C). Clinically
134 resistant bacteria (CIP ≥2ug/ml) did not arise in the three Lineages passaged in immunocompetent
135 mice. Furthermore, the number of bacteria able to survive on increased amounts of CIP relative to
136 the parental strain never rose above 0.1% of the population (survival on solid medium containing
137 1ug/ml CIP). Therefore, in immunocompetent mice, 15 passages were insufficient to allow
138 outgrowth and fixation of resistant variants in the population.

139 The evolutionary trajectories through neutrophil-depleted mice contrasted strongly with
140 immunocompetent mice, as the whole population in all three Lineages became CIP resistant over
141 the course of 15 passages. Bacteria resistant to at least 2 μg/ml CIP were observed as early as the
142 3rd passage (Fig. 2C). After the 9th passage, approximately $1x10^{-5}$ of the bacteria isolated from the
143 neutrophil-depleted mice showed resistance to 8 μg/mL CIP, four times higher than the clinically-
144 defined resistance breakpoint. By 15 passages, almost all bacteria from the neutrophil-depleted
145 Lineages were clinically defined as CIP resistant (at concentration of at least 2 μg/mL), with a large

146 fraction showing resistance to CIP =8 μg/ml. Therefore, resistance acquisition during disease is
147 amplified in the absence of neutrophils.

148 **Clinical failure results from a bacterial population that is clinically defined as drug**
149 **sensitive.** By the 6th passage in neutrophil-depleted mice, yields of bacteria began to approach
150 those observed in the absence of antibiotic (Fig. 1B), in spite of the fact that the majority of the
151 population remained sensitive to CIP based on the defined clinical breakpoint (Fig. 2C; clinical
152 breakpoint CIP>2 μg/ml). Yields remained high in successive passages, while the distribution of the
153 population increasingly skewed toward variants with increasing levels of resistance to CIP.
154 Therefore, drug treatment failure at passage 6 under neutrophil-depleted conditions was
155 dominated by bacteria that grew at 1μg/ml CIP but showed low viability at the 2μg/ml clinical
156 breakpoint. These mutants were replaced by more resistant isolates during later passages (Fig. 2C).

157 To link specific mutational changes over time to these observed phenotypes, we sequenced
158 the pools of genomic DNA isolated from the original inoculum, the parent AB17978 strain, and the
159 pools harvested after the 3rd, 6th, 9th, 12th and 15th passages. Mutation frequencies were then
160 plotted for each passage in the two immune conditions (Fig. 2B and 2D). Based on the predicted
161 sensitivity from the depth of pooled whole genome sequencing, we expected that only nucleotide
162 changes in greater than 5% of the population could be detected using this approach (Materials and
163 Methods).

164 The results from the pooled genomic sequencing allowed us to identify changes associated
165 with either the development of drug resistance, or the lack thereof, in these populations. As
166 predicted from Fig. 2A and the sensitivity limits of the analysis, there was no evidence for
167 mutations driving drug resistance at greater than 5% abundance in the three populations evolved
168 in immunocompetent mice. The only alteration that approached fixation was a mutation in a gene
169 encoding a putative solanesyl diphosphate synthase (ACX60_03850; *ispB*), but this allele was

170 unrelated to resistance, as single colony isolates showed no increased survival in the presence of
171 CIP (Fig. 2E). All the other mutations identified by sequencing the pools appeared unrelated to
172 resistance, as none survived incubation on solid medium containing 1μg/ml CIP (Figs. 2B, 2E).
173 Furthermore, the analysis of individual colonies isolated after plating bacterial populations on
174 antibiotic-free medium after the 15th mouse passage identified isolates with CIP MICs that were
175 only slightly elevated relative to the WT (Fig. 2E, left panel; WT MIC = 0.25-0.5).

176 Variants with altered CIP sensitivity arose in the immunocompetent mice, but they
177 remained at low levels in these populations, as predicted by the previous mathematical modeling
178 study (Fig. 2A) [18]. Mutations causing decreased drug sensitivity were identified by isolating single
179 colonies on solid medium containing 1μg/ml CIP, and all twelve of the single colonies selected from
180 the 10th passage had the identical mutation in *adeL*, the regulator of the AdeFGH egress pump [25,26].
181 The presence of the mutation in multiple Lineages is consistent with it existing in the initial
182 bacterial culture prior to the first inoculation of all three Lineages. Interestingly, 8 distinguishable
183 Lineage-specific strains were identified that were derived from the parental AdeL C312* mutation,
184 consistent with downstream mutations arising during mouse passage (Fig. 2E, right panel). These
185 strains appeared to be largely lost by passage 15 in the immunocompetent mouse (Fig. 2A, E). We
186 conclude that although strains with mutations that activate the AdeFGH egress pump are detected,
187 they are unable to overgrow the WT and are eventually depleted during later passages in
188 immunocompetent mice (Fig. 2B).

189 Consistent with the dynamic nature of resistance acquisition in neutrophil-depleted mice
190 (Fig. 2B), pool sequencing uncovered mutations that drove the stepwise trajectory to CIP^{R} in later
191 passages (Fig. 2D). Unlike the immunocompetent lineages, first step mutations that occurred within
192 *adeL* after 6 passages in neutrophil-depleted mice were easily detected by whole pool sequencing.
193 Each Lineage harbored different *adeL* mutations in these early passages that disrupted the 3' end of

194 the gene, consistent with previous work arguing that alterations in the C-terminus of the AdeL
195 protein result in AdeFGH pump activation[25,26]. Mutations in various other genomic sites arose
196 between passage 9 and 12, with many predicted to contribute to decrease susceptibility to CIP
197 treatment. For instance, the *adeL312** mutant acquired a second mutation in *gyrB* that overgrew
198 Lineage 1. In addition, a mutant harboring a noncononical mutation in *gyrA* arose in Lineage 2 that
199 was outcompeted by a strain with multiple genetic alterations, while a quadruple mutant appeared
200 to overgrow the single *adeL* mutant in Lineage 3.

201 To identify the various genotypes linked to increased CIP resistance, we isolated single
202 colonies after 9 passages to verify that two transiently predominant variants had the predicted
203 genotypes, and also sequenced isolates from passage 15 after plating in the absence or presence of
204 CIP (1μg/mL). Isolated colonies in absence of drug selection from Lineages 2 and 3 from passage 9
205 showed the predicted *adeL* alleles (compare Fig. 2D and 2F). In addition, after plating the passage
206 15 pools in the absence of drug, the two predicted gyrase alleles *gyrA*(A117E) and *gyrB*(Q447H)
207 that are observed infrequently in the clinic were also identified (Fig. 2F). Having *gyrA*(A117E)
208 alone was able to raise the CIP MIC by 16-fold (Fig 2F). Clones having the *gyrB*(Q447H) allele were
209 only observed linked to *adeL*(C312*) at passage 15, resulting in a CIP MIC that was 8-fold higher
210 than that of the parent strain (Fig 2E). Besides the mutations in target proteins, other single
211 colonies that resulted in a similar MIC increase were found to have a combination of four mutations
212 (Fig. 2F). When comparing the single colonies isolated that had a CIP of 1 μg/mL to those isolated
213 without antibiotic, the single colony isolates had genomic changes that were predicted by the
214 sequencing of the pools, indicating that the mutants described here became predominant without
215 requiring CIP selection *ex vivo*.

216 **Mutations in *adeL* allow for persistence in the presence of high levels of ciprofloxacin.**
217 To deconvolve the function of the various mutations observed, we backcrossed mutations into the

218 parent strain and assessed their relative contributions to CIP resistance. Of particular interest were
219 *adeL* nucleotide changes identified in populations after the 6th passage in neutrophil-depleted
220 mouse lineages, as CIP failed to efficiently restrict growth in the lung in these passages (Figs. 1A,
221 2D). The *adeL* gene (ACX60_06025)[26] has two predicted domains often associated with LysR type
222 transcriptional regulators: a helix-turn-helix domain and a substrate binding domain responsible
223 for regulation of the AdeFGH pump (Fig. 3A). Of the *adeL* mutations that arose during the *in vivo*
224 passages, one is located within the predicted substrate binding domain while the others are at the C
225 terminal end comprising in-frame deletions or early termination codons (Fig. 3A and 3B). We
226 constructed strains with each of these mutations and observed 100-1000X increased *adeG*
227 transcription levels compared to the parental strain, consistent with AdeFGH efflux pump
228 overexpression (Fig. 3C).

229 While these single *adeL* mutations resulted in an increase in MIC to ~1 μg/mL CIP that
230 barely rose to the level of significance (Fig. 4C), this level was below the recognized clinical
231 breakpoint[27], and such strains would be indicated as susceptible. As these are first step mutations,
232 we hypothesize that variants harboring these changes may facilitate the outgrowth of more
233 resistant isolates by promoting tolerance or persistence in the presence of antibiotic. To test this
234 model, we evaluated the survival of *adeL* mutants during exposure to high levels of CIP [28-32].
235 Exposure to 10 μg/mL CIP, roughly 20X MIC of the parental strain, led to the majority of the *adeL*
236 mutants (> 99%; MDK99) being rapidly killed (within 1 hour), mimicking what was observed for
237 the parental strain (Fig. 3D). However, unlike the parental strain, a subpopulation of the *adeL*
238 mutant was able to persist through 24 hours of drug exposure (Fig. 3D). This phenotype was
239 dependent on pump overproduction, as an *adeL* mutant strain deleted for the *adeFGH* operon was
240 indistinguishable from the parental strain in regards to persistence (Fig. 3D). These data argue that
241 *adeL* mutations drive persistence in the presence of CIP *via* increased expression of *adeFGH*,

242 providing a reservoir within neutrophil-depleted animals for the outgrowth of strains with
243 increased resistance[33].

244 **Resistance of evolved mutants in neutrophil-depleted mice can be explained by**
245 **combining *adeL* with *mfsA* mutations.** We continued backcross analysis to identify the minimal
246 determinants necessary to confer clinical resistance during passage in the mouse. Many of the single
247 colony isolates from Lineage 3 at passage 15 of the immunocompromised mice possessed a
248 combination of mutations in four genomic locations: *adeL*, *acfR* (ACX60_03155), *lpxD*, and the
249 intergenic *rpmL-mfsA* region, the latter of which is located between a ribosomal protein gene and a
250 predicted coding region for a putative MFS transporter which we have named *mfsA* (ACX60_15150,
251 annotated as *nreB* in GenBank; Fig. 2D and 2E). To determine the role in drug susceptibility of each
252 of these mutations, we constructed separate strains carrying single mutations. All single mutants
253 showed various MICs well below 2 μg/ml CIP, with each of the *adeL* mutations as well as *mfsA*(-9)
254 showing increased MICs above the parental strain (Table S1; Fig. 4C). The *mfsA*(-9) mutation is
255 located 9 bp upstream of a predicted MFS efflux pump, within 2 bases of a previously reported
256 mutation selected during evolution of CIP resistance in *A. baumannii* in planktonic conditions[34].
257 Consistent with MFS transporter over-production, we found that the *mfsA*(-9) mutation increased
258 the *mfsA* mRNA levels by ~9-fold relative to the parental strain, based on q-rtPCR analysis (Fig. 4B).
259 Significantly, when the *mfsA*(-9) mutation was combined with the *adeL*P131H mutation, the CIP MIC
260 increased to ~4ug/ml approaching that of the quadruple mutant strain isolated from mouse passage
261 15 (Fig. 4C; Table S1). A single nucleotide change located nearby the *mfsA*(-9) mutation that arose
262 transiently in the immunodepleted Lineage 3 (Fig. 2D; *mfsA*(-19)) behaved nearly identically (Figs.
263 4B,C). Therefore, combining two mutations that resulted in upregulation of both the AdeFGH pump
264 and a putative MFS transporter was sufficient to provide CIP resistance above the clinical
265 breakpoint, approaching that seen for the quadruple mutant.

266 **A hotspot for mutations within *lpxD* is tightly linked to fluoroquinolone resistance in**
267 **clinical isolates.** The mutation *lpxD* T118_A119insA (locus tag: ACX60_07955; GenBank:
268 AKQ26661.1) was consistently found in CIP^R isolates from mice. This alteration within an
269 acyltransferase involved in lipooligosaccharide (LOS) biosynthesis[35-37] showed no effect on MIC
270 (Table S1). To test for clinical linkage of *lpxD* mutations to drug resistance, we downloaded the
271 genomes of all 8666 *A. baumannii* genomes clinical isolates from the PATRIC database[38]. Focusing
272 on nonrepetitive sequences that had antibiotic resistance profiles, 1830 were resistant to
273 ciprofloxacin and 215 were susceptible. Of the CIP^R isolates, 883 genomes had an E->K change at
274 residue number 117, with a *z*-score $\geq$ 18 (Supp. Fig. 1). In comparison, only 9 of 215 CIP^S isolates
275 had the same mutation. By Fisher's exact t test, $p<0.0001$, supporting the siginificance of these
276 observations.

277 To determine if the overrepresentation of the E117K allele could be due to outgrowth of a
278 single clone, we performed multi-locus sequence typing (MLST) using the Pasteur *A. baumannii*
279 scheme, generating 7-gene allele profiles [39]. Of the 123 distinct MLST groups, 16 had both CIP^R and
280 CIP^S isolates (Supp. Dataset 1; Supp. Fig. 2), although over half of the CIP^R isolates belonged to two
281 MLST types (ST2 and ST3). To avoid skewing the results due to this overrepresentation, we limited
282 the number of isolates per ST group to 1, reducing strains analyzed to 139 across 123 distinct MLST
283 groups (Fig 5A), including 59 CIP^R isolates and 80 CIP^S. Even after limiting the clonal effects in this
284 fashion, we still observed overrepresentation, with the E117K allele found in 13 of 59 CIP^R isolates
285 (Fig. 5B), while only 3 of 80 CIP^S isolates had the same alterations (Fig. 5B; $p= 0.0011$, Fisher's exact
286 t test). Both a whole genome phylogenetic tree (Supp. Fig. 3) and clustering analysis of the 7-gene
287 allelic profiles from these 139 clinical isolates (Fig. 5C) identified CIP^R isolates that shared parents
288 with CIP^S ones, further arguing against clonal effects for the enrichment.

289 Interestingly, the alteration at residue E117 (z-score: 8.98; p-value, < 0.00001) directly
290 proceeds the T118 allele identified in our mouse experiments, with both variants predicted to be in
291 a turn between two beta sheets (Fig. 5D)[38]. Although the significance of this linkage is unclear, the
292 fact that the *lpxD* T118_A119insA has a fitness defect in broth (Fig. 5E), raises the possibility that
293 mutations in this turn could contribute to a persistence phenomenon in tissues leading to evolution
294 of drug resistance.

295 **Evolutionary replay experiments reconstruct the pathway to drug resistance.** The
296 observation that resistant organisms outcompeted a persistent strain (Fig. 2D) could be due to a
297 coincidence that occurred during serial passage or due to antibiotic-driven selection for strains
298 with increased MIC over persistent strains. We performed three evolutionary replay experiments[40]
299 with neutrophil-depleted Lineage 3 variants to distinguish between these possibilities. In the first
300 (Fig. 6A), bacteria were harvested after passage 9 and cycled 3 times in duplicate in neutrophil-
301 depleted animals to test if the AdeL ΔI335A336 allele, a 6 nucleotide in-frame deletion identified in
302 cyclophosphamide treated animals, would again be outcompeted by low abundance drug-resistant
303 mutants (Fig. 2D). The second approach was to passage three times a mix of a colony-purified drug
304 persistent AdeL ΔI335A336 single mutant (P9Cy3.1; Table S1) with a colony-purified drug resistant
305 quadruple mutant (Cy31; Table S1) in the approximate ratio present at passage 9 (95:5; Fig. 6B).
306 The third was to test the model that neutrophils restrict the outgrowth of strains having activating
307 mutations in *adeL* (Fig. 6C).

308 When the *adeL* mutant was analyzed in competition within the pool (Fig. 6A) or when
309 mixed 95:5 with colony purified quadruple mutant (Fig. 6B), we observed an increase in bacterial
310 burden and fraction of bacteria showing CIP MIC >2 after passaging the pools in neutrophil-
311 depleted CIP-treated mice (Supp. Fig. 4). Whole genome sequencing of the bacterial populations
312 harvested after each passage revealed a near identical evolutionary trajectory as seen from the

313 original experiment, with the single mutant associated with drug persistence eventually
314 outcompeted by drug resistant mutants (Fig. 6). Furthermore, in one of our replicate Lineages (Fig.
315 6A), another mutation located in the intergenic region between *rpmL* and *mfsA* (*mfsA*(-19)) arose
316 that had appeared transiently in immunodepleted Lineage 3 (Fig. 2D), further arguing for the
317 contribution of this regulatory region in resistance evolution. Therefore, these two reconstructions
318 (Figs. 6A,B) demonstrate that the evolutionary trajectory is reproducible, and can be regenerated
319 by phenotypically similar mutations that arise spontaneously.

320 In the third experiment, single *adeL* mutants were unable to overgrow the WT in the
321 presence of CIP in immunocompetent animals, in contrast to what was observed in passage 9 of the
322 neutrophil-depleted animals. When a 5:95 (*adeL*:WT) mixture was passaged in immunocompetent
323 mice, the mutant was unable to increase its population share (Fig. 6C), mimicking the failure of *adeL*
324 activating mutations to overgrow the pool in any of the immunocompetent Lineages (Fig. 2A). In
325 contrast, CIP^R mutants having canonical resistance alleles in *gyrA* or *gyrAparC* were able to compete
326 efficiently with WT in the presence of neutrophils, with the GyrA(S81L) ParC(S84L) double mutant
327 growing from 5% to 70% of the population within 3 passages (Fig. 6C). This argues that depleting
328 the immune response allows the outgrowth of persistence mutants, facilitating complex pathways
329 to drug resistance that are blocked in immunocompetent hosts.

330 **Ciprofloxacin treatment within the host simultaneously selects for increased**
331 **resistance and enhanced fitness.** Antibiotic resistance is often associated with a fitness cost[41] that
332 may be compensated over time by continued selection of secondary genotypes that overcome these
333 costs. The inability of the *adeL* mutant to overgrow WT during infection in the presence of CIP in
334 immunocompetent animals may reflect this point. Mutants with high resistance, however, could
335 maintain their selective advantage over non or low-resistance mutants even in the absence of drug
336 treatment. To test this model, the relative fitness of the drug resistant mutants derived from

337 neutrophil-depleted Lineages was compared to the parent strain AB17978. In the absence of CIP,
338 variants isolated after passage in neutrophil-depleted mice showed varying degrees of subtle
339 growth impairment in broth relative to the parental strain (Fig. 7A; Cy11, $p < 0.01$). During animal
340 infections in the absence of antibiotic, these growth defects were amplified. When
341 immunocompetent mice were challenged with the high fitness *gyrAparC* mutant in competition
342 with the WT, the two strains showed similar levels of colonization (Fig. 7B). In contrast, each of the
343 drug resistant mutants derived from neutrophil-depleted mice competed poorly in
344 immunocompetent animals (Fig. 7B; $p < 0.0001$).

345 Although the lowered fitness of mutants in immunocompetent animals further supports
346 the model that outgrowth of unique resistance alleles occurs in the absence of neutrophils, it did
347 not directly test the model that selection in neutropenic mice increased fitness relative to first-step
348 CIP^R variants. In the absence of CIP treatment, the parent strain showed a subtle advantage over the
349 Lineage 3 quadruple mutant isolate Cy31 (Table S1) under neutrophil-depleted conditions,
350 although the results were clearly not as robust as in the presence of neutrophils due to increased
351 scatter (Fig. 7C; Cy31 against WT). More striking is the fact that the Cy31 strain had a clear fitness
352 advantage over its predecessor, the Lineage 3 *adeL* mutant, when competed in the absence of
353 antibiotics (Fig. 7C; Cy31 against P9Cy3.1). Therefore, in competition with persister mutants,
354 ciprofloxacin simultaneously selected for an isolate with increased CIP resistance and enhanced
355 fitness relative to mutant competitors. This predicts that drug-resistant mutants were able to
356 evolve to heightened fitness to replace persister mutants. As fitness increases, resistant mutants
357 should be able to compete with sensitive strains even after cessation of antibiotic treatment,
358 potentially escalating treatment failure and providing fertile ground for the emergence of resistant
359 strains with high fitness.

360

361 # Discussion

362 Comparative analyses of bacterial pathogen databases indicate that clinical antibiotic
363 resistance is associated with mutations located outside well-characterized drug targets [20-22].
364 Analysis of clinical resistance is often retrospective, with a few exceptional studies that have
365 allowed identification of a timeline of bacterial resistance in human populations[28-32,42-44]. Our study
366 bridges an important gap in understanding how resistance evolves, by following experimental
367 evolution of fluoroquinolone resistance in a pneumonia disease model. Strikingly, in the absence of
368 one arm of immune pressure, *A. baumannii* resistance arose after few passages in murine lungs
369 during CIP treatment (Fig. 1B), resulting in treatment failure. Conversely, the overall frequency
370 remained low in immunocompetent mice, and this did not lead to treatment failure (Fig. 1B).

371 The absence of neutrophils resulted in the identification of rare alleles associated with drug
372 resistance. In contrast to the canonical target site GyrAS81LparCS84L mutation which shows high
373 fitness under conditions tested, the *gyrA*A117E and *gyrB*Q447H alleles rarely observed in clinical
374 strains predominated in two of the lineages from neutrophil-depleted animals (Fig 2E). These
375 unusual isolates showed fitness defects during disease and/or in culture (Fig. 7) that make them
376 unlikely to arise in the presence of intact immune functions, consistent with evolutionary
377 trajectories being determined by the immunological state of the host. Therefore, we propose that
378 immunocompromised hosts are incubators for the generation of unique drug resistant variants,
379 with uncertain outcomes after pathogen exposure to the community at large. Although the variants
380 we described have reduced fitness relative to WT, continued passage demonstrated that stepwise
381 increase in drug resistance was associated with stepwise increase in fitness (Fig. 7). Similar fitness
382 effects have been obtained during continued passage in culture[34]. The recent demonstration of
383 enhanced viral evolution of SARS-CoV-2 in an immunocompromised patient undergoing
384 therapeutic antibody treatment is a graphic example of the potential interplay between immunity,

385 antimicrobials and evolution in the clinic, with potential largescale community effects[45].
386 Furthermore, persistence mutants have been demonstrated to arise during continued antibiotic
387 therapy in an immunocompromised patient treated for vancomycin-resistant enterococcus[46], tying
388 the results presented here with documented clinical outcomes.

389 Antibiotics primarily act by targeting essential cellular functions or pathways [47,48]. In
390 response to transient antibiotic exposure, a proportion of bacteria typically persist or tolerate this
391 treatment with mutations arising that can increase the fraction of the surviving population[49-51]. The
392 mechanisms for allowing persistence/tolerance likely differ between bacterial species and vary
393 among antibiotics[52], but it is generally agreed that persistence/tolerance is caused by cell
394 dormancy[53-55] or transient expression of efflux pumps and stress response pathways[28,56].
395 Persistence/tolerance mechanisms may play an important role in the relapse of bacterial infections
396 [57-59]. In our study, we found that persistence in *A. baumannii* can be promoted by upregulation of a
397 drug efflux pump, AdeFGH [26]. It is known that clinical isolates often overproduce efflux pumps that
398 remove multiple antibiotics from the bacterial cytoplasm[26,60], and that antibiotic persistence is
399 associated with such pump upregulation[61,62]. Of note, mutations upregulating this pump are rarely
400 isolated in the laboratory through simple antibiotic single-step selections on solid agar, indicating
401 there may be a special environment in the lung that allows outgrowth of these mutants.

402 There are three important repercussions from the analysis of the AdeL efflux overproducer
403 mutations. First, overproduction results in drug treatment failure during pneumonic disease in the
404 mouse, in spite of the fact that these bacterial strains are CIP-sensitive based on the international
405 standard for clinical breakpoints[27]. Therefore, clinical drug treatment failure in the absence of
406 identified antibiotic resistance[9] could be explained by the outgrowth of drug persistent mutants,
407 particularly in the immunocompromised host. Second, the *adeL* mutations provide a molecular
408 basis for *A. baumannii* to develop second-step variants that lead to CIP resistance above the clinical

409 breakpoint. Of interest, inhibitors of efflux pumps have been suggested to re-sensitize bacteria to
410 multiple antibiotics[63], but perhaps such a regimen may also delay progression to resistance. Finally,
411 isolates from drug treatment failure occurring in immunocompromised patients could generate a
412 pool of precursor mutants giving rise to resistant isolates that eventually infect a broad range of
413 patients. A number of studies have similarly argued that efflux pump mutations provide a critical
414 pool for the multi-step evolution of antibiotic resistance [33,64,65]

415 We propose a model of bacterial resistance progression in immunodepleted hosts (Fig. 8).
416 When infecting a host, the antibiotic susceptible bacteria colonize at a relatively low rate. With
417 active transmission and continuous CIP treatment, there is outgrowth of bacterial persisters that
418 have MICs below the clinical breakpoint, increasing the bacterial load at the infection site. On
419 continued treatment, or transfer to a similar host undergoing CIP treatment, fully resistant mutants
420 can then outgrow the population. The presence of intact immune function interferes with
421 outgrowth of these mutants, but the identification of persister mutants in the presence of immune
422 function indicates that such alleles could act as enablers of drug resistance in all hosts, particularly
423 under conditions of temporary breaching or depression of innate immunity.

424 Genomic analyses can identify allelic variants linked to drug resistance, but verifying the
425 functional importance of these alleles is hindered by founder effects that are often difficult to
426 discount. The *lpxD* E117K mutation is one such allele associated with resistant *gyrA* S81L-
427 containing genomes. The fact that the adjacent *lpxD* T118 insA allele was isolated during multiple
428 passages in immune-depleted mice argues for a role of these altered residues in supporting the
429 outgrowth of drug resistant organisms. The *lpxD* T118 insA mutation likely alters envelope
430 function. This raises the possibility that the mutation causes subtle changes in permeability that
431 slow drug access to target, or else the slowed growth of strains harboring this allele increases drug
432 tolerance during growth in tissues[52]. Our inability to demonstrate increased tolerance to CIP and

433 the fact that the clinical *lpxD* E117K did not show a fitness defect when grown in LB broth (Fig. 5E)
434 argues that the critical phenotypes may be observed exclusively during growth in tissues, making
435 them difficult to evaluate.

436 In summary, we hypothesize that resistance progression in clinical isolates follows a similar
437 trend witnessed in our experiments, albeit with greater complexity in the human. Drug sensitive
438 bacteria may colonize both healthy and immune system-compromised patients, but resistance
439 evolution occurs more rapidly within hosts having impaired neutrophil function. The canonical
440 resistance mutations that arise within healthy individuals may compete efficiently with host-
441 evolved mutations in patients having impaired neutrophil function. Hence, the transmission from
442 individuals having intact immune function may pose risks to immunocompromised patients.
443 Adding to the risks subjected to vulnerable patients, we found that *A. baumannii* persistence
444 mutants with MIC levels below the clinical breakpoint were associated with treatment failure,
445 emphasizing the difficulty in treating these patients (Fig. 1B) [9,66-69]. While heterogeneity and
446 variability between infected patients is inevitable, this work provides insight into some genetic
447 factors that could predispose individuals to treatment failures in specific clinical contexts. Future
448 work should be focused on how this evolutionary trend towards drug resistance can be controlled,
449 such as tackling the molecular basis for selection of persister or other mutations that lead to
450 treatment failure.

451 # Material and Methods

452 **Bacterial Strains.** Bacterial strains used in this study are listed in Table S1. *Acinetobacter*
453 *baumannii* strains are derivatives of ATCC 17978. Bacteria were grown in Lysogeny Broth (LB) (10
454 g/L tryptone, 5 g/L yeast extract, 10 g/L NaCl) or on LB agar plates (LB supplemented with 15g/L
455 agarose). Broth cultures were grown at 37°C in flasks with orbital shaking at 200 rpm or in tubes
456 with rotation on a roller drum at 56 rpm. Growth was monitored by measuring absorbance
457 spectrophotometrically at 600 nm (A_{600nm}). Plates were incubated at 37°C. Antibiotics were used at
458 the following concentrations: Gentamicin: 10 μg/mL (*A. baumannii*) and 50 μg/mL (*E. coli*);
459 Carbenicillin: 100 μg/mL.

460 **Murine experimental evolution.** The *in vivo* passaging experiments were performed
461 identically in either immunocompetent or neutrophil-depleted 6-8 weeks-old female BALB/C mice
462 (Fig. 1A). Neutrophil depletion was induced via cyclophosphamide pretreatment [70]. Briefly, 150
463 mg/kg and 100 mg/kg of cyclophosphamide monohydrate (Sigma-Aldrich: C7397) were
464 administered 4 days and 1 day prior to infection, respectively. At the time of infection, mice were
465 transiently anesthetized by inhalation of isoflurane and lung infections were established using ~10^8
466 colony forming units (CFU) of *A. baumannii* from mid-log phase cultures (A_{600nm} ~0.5) via
467 oropharyngeal aspiration [71]. For Passage 1, all Lineages were derived from a single broth-grown
468 culture. At 7 and 19 hours post infection (hpi), 100 mg/kg of ciprofloxacin (Sigma-Aldrich:
469 PHR1044) was administered via subcutaneous injection. At 27 hpi, mice were euthanized, and
470 lungs were removed aseptically and homogenized in 1 mL of ice-cold 1x phosphate buffered saline
471 (PBS). Afterwards, the homogenate was plated on large (150 x 15 mm) LB agar plates and
472 incubated for ~17 hours at 37°C. The total number of bacteria was quantified using CFU. The
473 enriched bacteria were scraped off the LB plates and resuspended in 1x PBS. The resuspension was
474 used for DNA isolation as well as the inoculum for the next passage/round of infection (stored at -

475 80°C in 20% glycerol prior to use). For each round of mouse infection/passage, bacterial frozen
476 stocks were revived by diluting them in LB broth and growing them to exponential phase.
477 Afterwards, ~10^8 CFU of the pool was used to establish infection in each mouse. Three separate
478 Lineages of murine infections were maintained in parallel in each condition (immunocompetent or
479 neutrophil depleted), and within each Lineage each starting inoculum was passaged 15 times.
480 Validation experiments involving the reconstruction of identified mutants and re-passaging of these
481 strains in mice were similarly performed.

482 **Murine Competition Assays.** Competition experiments were performed as described
483 previously[71]. Briefly, designated strains were grown to exponential phase (A_{600nm} ~ 0.5-1.0) and
484 mixed at a 1:1 ratio for the inoculum. Afterwards, ~10^8 CFU of the bacterial mixture was used to
485 challenge WT or cyclophosphamide-treated BALB/C mice via the oropharyngeal route as described
486 for the mouse passage experiments. 24 hr post inoculation, lungs were removed aseptically,
487 homogenized and extracts were spread on LB agar plates. To quantify the input and output ratio of
488 each designated strain, both the inoculum and the lung homogenate were serially diluted in 1x PBS
489 and plated on LB agar as well as LB agar supplemented with 2 μg/mL of ciprofloxacin to
490 differentiate between the WT and CIP resistant test strains. Selection rate coefficients (SRC) were
491 determine by SRC = ln(Strain 1 output/input ratio) – ln(Strain 2 output/input ratio)[72]. Prism was
492 used for statistical analysis and significance was determine by one-way ANOVA followed by
493 Dunnett's or Tukey's Multiple Comparison. *$p<0.05$; ****$p<0.0001$.

494 **Evolutionary replay experiments.** For the evolutionary replay experiments (6A), the
495 saved Cy3 Passage 9 pool was used as inoculum. For the evolution experiments involving isolates
496 (Figs. 6B and 6C), designated strains were grown to exponential phase and mixed at a 5:95 ratio in
497 the inoculum. In both cases the inoculum was administered via the oropharyngeal route to mice
498 and passaged three times in the presence of CIP treatment in a near identical manner as the initial

499 passaging experiments. Each pool/mixture was performed in duplicate. The bacterial pools after
500 each passage were saved, and variant frequencies at each passage were determined as described
501 above. The abundance of each mutant in the isolate mixtures was determined by measuring the
502 colony forming efficiency (CFE) at an antibiotic concentration that was below the mutant MIC but
503 above that of wild type AB17978. The CFE versus passage number was displayed and expressed as
504 strain abundance (%). CFE = number of colonies on antibiotic-containing medium / number of
505 colonies in the absence of antibiotic.

506 **Determining the fraction of resistance as a function of ciprofloxacin concentrations in**
507 **each pool**. To evaluate the fraction of bacteria acquired from each passage that are viable on
508 culturing in various concentration of ciprofloxacin, the glycerol stock of each pool was revived in
509 fresh LB broth and grown to exponential phase. A total of ~10^7 CFU were used for serial dilutions in
510 1x PBS and 10 μl from each diluted culture was spotted on LB agar plates containing the following
511 concentrations of ciprofloxacin: 0, 0.25, 0.5, 1, 2, 4 and 8 μg/ml. After an overnight incubation at
512 37°C, colonies were counted, and CFU/ml was calculated. A detection limit of 100 CFU/ml was used.
513 The fraction bacteria resistant to a certain concentration (C_0; $C_0 > 0$) of ciprofloxacin is calculated as
514 (CFU/ml at C_0 - CFU/ml at all concentrations above C_0) / Total CFU. A stacked bar plot of the data
515 was generated using Prism GraphPad (Fig. 2).

516

517 **Whole Genome Sequencing.** Genomic DNA (gDNA) was extracted from bacteria using the
518 DNeasy Blood and Tissue kit (Qiagen). Library preparation was performed using Illumina Nextera
519 with previously described modifications [73]. Libraries were enriched with 8 cycles of PCR and
520 sequenced using HiSeq2500 at Tufts University Core Facility using single-end 100 bp reads. Reads
521 were aligned to the *A. baumannii* ATCC 17978 genome and its plasmids (GenBank Accession:
522 CP012004; pAB1: CP000522; pAB2: CP00523; pAB3: CP012005), and variants were identified at

523 5% cutoff using breseq 0.32 [74]. Reads were aligned to *A. baumannii* ATCC 17978 reference genome
524 (https://genomes.atcc.org/genomes/e1d18ea4273549a0) to include an additional 44kb gene
525 cluster [75]. The identified mutations are listed in Supplemental Dataset 2. The predicted functional
526 impact of substitution variants was determined by using PROVEAN [76].

527 **Persistence Assay.** *A. baumannii* was grown in 3 individual LB broth cultures overnight
528 from separate colonies. The cultures were diluted 1000-fold into 8 ml LB broth and incubated by
529 rotation at 37°C for 2-3 hours until reaching mid or late exponential growth (A_{600nm} ~ 0.3-0.8).
530 Ciprofloxacin was added to reach a final concentration of 10 μg/ml, the concentration regarded as
531 20x the MIC for the parent ATCC 17978 *A. baumannii* strain. These cultures were then incubated at
532 37°C for up to 24 hours. After 0, 1, 3, 6, and 24 hours, 500 μl of culture was removed, washed twice
533 in 1x PBS, resuspended in 500 μl PBS, and sequentially diluted in 1x PBS. Serial dilutions were used
534 for CFU quantification by spot plating on LB agar plates. Dilution factors harboring quantities
535 ranging from 3-35 CFUs were used to calculate the CFU/ml. The limit of detection by this assay was
536 determined to be 375 CFUs. The CFU/mL across the biological replicates at each time point
537 throughout the drug challenge were plotted as mean ± Standard Error of Mean.

538

539 **qRT-PCR gene expression analysis.** Bacteria were grown to early stationary phase in LB
540 broth, RNA was harvested and purified using RNeasy kit (Qiagen) followed by cDNA synthesis using
541 SuperScript VILO cDNA kit (Thermo Fisher). The cDNA was then amplified with PowerUp SYBR
542 Green Master Mix (Applied Biosystems) via a StepOnePlus Real-Time PCR system (Applied
543 Biosystems) per manufacturer's instructions, and target amplification efficiency was evaluated by
544 generating a standard curve with dilutions of cDNA (>95% amplification efficiency for each primer
545 pair). Primers were designed to amplify regions of around 150 bp internal to genes (Table S2).
546 Triple technical replicates were examined per biological sample and at least three biological

547 replicates per strain were tested, with controls lacking reverse-transcriptase included to verify a
548 lack of contaminant genomic DNA. Transcript levels of specific targets from each strain were
549 evaluated by the comparative $2^{-\Delta\Delta Ct}$ method to the parental strain, normalizing to that of the
550 endogenous control 16s. The transcript level for each target across biological replicates was plotted
551 as mean ± Standard Error of Mean (Fig. 3&4).

552

553 **MIC determination.** Minimum inhibitory concentrations (MICs) were determined by broth
554 microdilution. Overnight cultures of strains of interest were diluted 1000X in fresh LB broth and
555 grown to mid-logarithmic phase (A_{600} ~0.5). Afterwards, cultures were diluted to a final A_{600} =
556 0.003 and tested in the presence of two-fold dilutions of antibiotics. 200 μl of culture-antibiotic
557 mixture was then aliquoted to a 96 well plate (COSTAR) and technical duplicates were performed in
558 a Biotek plate reader with rotation. Growth was monitored by measuring A_{600} at 15 min. intervals
559 for 16 hr, and the MIC was determined as the lowest concentration of drug that prevented growth,
560 using at least three biological replicates for each strain. The MICs across biological replicates were
561 plotted as mean ± Standard Error of Mean (Fig. 4).

562

563 **Molecular cloning and mutant construction.** Plasmids and primers used in this study are
564 listed in Table S2. The mutant strains were constructed through sequential cloning into pUC18[77]
565 then pJB4648[78] as previously described[13]. Briefly, the mutant allele from each strain of interest was
566 amplified alongside upstream and downstream segments to generate a PCR product ~1500 bp in
567 length flanked by appropriate restriction sites. The PCR product was then ligated into pUC18 and
568 propagated in *E. coli* DH5α. The PCR product was then subcloned from pUC18 into pJB4648 and
569 propagated in *E. coli* DH5α λpir. After sequence confirmation, the pJB4648 plasmid construct

570 containing the desired mutation was introduced into *A. baumannii* via electroporation. Markerless,
571 in-frame mutations were isolated via homologous recombination as described [13].

572

573 **Comparative sequence analysis.** Genome sequences from 8666 *A. baumannii* clinical
574 isolates and ciprofloxacin resistance profiles for 2618 isolates were downloaded from PATRIC
575 database in Nov 2021 as described in results. MLST analysis was performed using Pasteur scheme[39]
576 with the publicly available tool "mlst" (https://github.com/tseemann/mlst). The LpxD protein
577 sequence from ATCC 17978 was compared to these 2045 isolates using tblastn to identify the
578 amino acid locations of mismatches and gaps. The nucleotide sequences with the best matches to
579 the LpxD protein were extracted and translated into protein sequences. For each isolate, the
580 translated LpxD sequence was compared to the reference LpxD sequence from AB17978. The
581 nonsynonymous changes were recorded for each clinical isolate. The nonsynonymous changes at
582 each residue were then summarized to reflect the total number of clinical isolates showing those
583 changes. The raw numbers were further transformed into *z*-scores to determine if a particular
584 residue was significantly overrepresented by nonsynonymous changes linked to CIP^R or CIP^S
585 phenotypes (Supp. Fig. 1). In order to reduce clonal effects, one clinical isolate per ST group was
586 selected randomly. Multiple aligned LpxD protein sequences are shown in Supp. Dataset 3. One
587 isolate had no hit for LpxD. The MLST profiles from 7 housekeeping genes were used to calculate
588 the Euclidean distance, and hierarchical clustering was determined using R (Fig. 5A). A
589 phylogenetic tree from these 139 genomes was built using mashtree [79] and visualized in Geneious
590 Prime (https://www.geneious.com/) (Supp. Fig. 3). The presence and absence of isolates was
591 summarized and visualized in a heatmap using Prism GraphPad v9 (Fig. 5B; Supp. Fig. 2). Within
592 each group, the mismatches/gaps at each amino acid location within LpxD were displayed as
593 number of genomes having mismatches/gaps at that location. A table of the data was constructed

594 showing the specific amino acid in the rows, the genome groups harboring these mutations in the
595 columns, and the total number of mismatches/gaps in the cells. The results in each cell were then
596 normalized using *z*-scores with the mean and standard deviation from individual genome groups.
597 The *z*-score was plotted as function of each residue.

598

599 **Calculation of doubling time in broth culture.** Overnight cultures of bacteria were diluted
600 1000-fold in fresh LB broth and grown for 8 hours. The A_{600} values were measured every hour
601 using a spectrophotometer, and the log2 transformed values were plotted as a function of time (hr).
602 To calculate the doubling time, a modified sigmoid function ($y = \frac{L1}{e^{-k(x-x0)}+1} - L2$) was fitted to the
603 plotted curve (y: log2 transformed A_{600} value, x: time in hrs, x_0: timepoint when the growth rate was
604 the fastest, k, L1, L2: rate constants), with the fastest growth rate for each culture determined as the
605 time in which second derivative of the fitted curve approached 0 (or when $x = x0$), at which point
606 the doubling time was represented as the inverse of the slope ($\Delta t = {}^{4}/_{k * L1}$) (Code available at:
607 https://github.com/huoww07/calulate_bacteria_doubling_time). To evaluate the goodness-of-fit,
608 the R^2 value was calculated for each growth curve assay (the R^2 ranges from 0 to 1, representing the
609 worst to the best fit). At least three biological replicates were performed for each test strain (Table
610 S3, Table S4) and the average doubling time and standard deviation was calculated. Statistical
611 significance was performed using one-way ANOVA followed by Dunnett's multiple comparisons.

612

613

614 # Accession numbers.

615 The datasets generated during the current study are available in the Sequence Read Archive
616 (PRJNA485355). Detailed accession numbers for each sample are listed in Table 1.

617

618 # Acknowledgements

619 This work is supported by NIAID U01AI12430 to TvO, JWR, VSC and RI, NIH R21AI128328 to RI and
620 T32AI07422 support for JH-B. We thank the colleagues in all of our labs for support and constant
621 critiquing of the experimental strategies used here. We thank all anonymous reviewers for critical
622 comments and suggestions.

623

624 # Author Contributions

625 RI, JR and TvO devised the study. LB, JH and WH performed the mouse experiments. WH, EH and JH
626 performed the wet-lab experiments. WH and LB performed the whole genome sequencing and
627 bioinformatics analyses. CM, VC, EG and TvO collaborated on the bioinformatics analyses and
628 performed training. WH, LM, EH, JH and RI interpreted the results and wrote the manuscript. WH,
629 LB, EH, JH, CM, EG, VC, TvO, JR and RI approved the final manuscript.

630

631 # Figure Legends

632 **Figure 1. Continuous passaging of *A. baumannii* in a lung infection model results in early**
633 **antibiotic failure in neutrophil-depleted mice.** A). The 15-passage strategy using the pneumonia
634 model in both immunocompetent and neutrophil-depleted mice. Neutrophil depletion was induced
635 by two doses of cyclophosphamide at 72- and 24-hrs prior of infection. At the time of infection, *A.*
636 *baumannii* ATCC 17978 was oropharyngeally inoculated into mice at 10^8 CFU, and two doses of CIP
637 were administered at 9- and 19-hrs post infection. All Lineages are derived from a single broth-
638 grown culture. At 27-hrs post infection, the mice were euthanized, lungs were homogenized, and
639 bacteria were plated on LB agar plates. After overnight growth, the bacteria were collected and 10^8
640 CFU used for the next round of infection/passage. B). Rapid development of antibiotic failure as a
641 consequence of passage in the absence of neutrophils. After lungs were homogenized, total CFU on
642 LB agar in the absence of antibiotic were determined and plotted as function of passage number.
643 Shown are three lineages for immunocompetent and neutrophil-depleted animals treated with CIP
644 as described in panel (A).

645

646 **Figure 2. High level ciprofloxacin resistance evolves in a stepwise fashion during passage in**
647 **neutrophil-depleted mice.** (A, C) After each passage, bacteria from lung homogenates were
648 serially diluted onto LB agar containing noted concentrations of CIP (μg/ml). The fraction of CFU on
649 the series of CIP plates was determined for each pool and displayed in stacked bar plots for immune
650 competent (A) and immune depleted (C) mouse infection Lineages. The limit of detection was 2.7E-
651 6. (B, D) The gDNA from each bacterial pool was isolated and subject to whole genome sequencing
652 to identify the genomic mutations acquired throughout passaging (after passage 3, 6, 9, 12 and 15).
653 The mutations were detected using a 5% abundance cutoff and filtered against the parent strain

654 AB17978. The relative abundance of each mutation was plotted as a function of passage number
655 from (B) immune competent Lineages and (D) immune deficient Lineages (D). (E-F) After 10 or 15
656 passages (as noted), the bacterial pools from each Lineage were incubated on LB in the presence or
657 absence of CIP (1 μg/mL) to select for single colonies. Purified single colonies were subjected to
658 whole genome sequencing and MIC assays. In (E-F), each column represents a single colony. Rows
659 display absence or presence of selection criteria, passage, amino acid or SNP alleles, and MIC values
660 for each single colony isolate. The presence of each mutation in an individual colony is highlighted
661 in purple. MICs are labeled and color-coded for all colonies, a minimal of three biological replicates
662 were performed.

663

664 **Figure 3. *adeL* mutations drive bacterial persistence through over-expression of the AdeFGH**
665 **pump.** (A). Sites of nonsynonymous changes during *in vivo* passaging and domain structure of
666 AdeL. (B). Locations of nonsynonymous changes on predicted functional domains of AdeL. (C).
667 Mutations in *adeL* selected during mouse passage result in specific overproduction of an AdeL-
668 regulated gene *adeG*. Data were determined by qRT-PCR analysis of pump-encoding components
669 *adeG* (regulated by AdeL) or *adeB* and *adeJ* (components of other pumps) in noted *adeL* mutant
670 backgrounds. (D). Overproduction of AdeL-regulated pump components results in increased
671 persistence in presence of CIP. AB17978 derivatives described in legend were exposed to CIP at
672 20X MIC for noted times and titered for viability by quantitating CFUs. Data shown are mean ±
673 Standard Error of Mean, a minimal of three biological replicates were performed.

674

675 **Figure 4. The presence of mutations in *adeL* and *mfsA* is sufficient to explain CIP^R in strains**
676 **derived from mouse passage experiments.** A) Two mutations located directly upstream of *mfsA*
677 selected during mouse passaging experiments. B) Transcription levels of *mfsA* and *rpmL* were

678 determined by qRT-PCR in strains harboring the two mutations upstream of *mfsA*. Significance
679 level: ****, $p < 0.0001$ using two-tailed t-test against mean fold change of WT. Two technical
680 replicates and at least three biological replicates were performed. Data are mean MICs ± SEM. C)
681 Double mutants containing *adeL* and *mfsA* mutations show MICs of CIP that are similar to evolved
682 quadruple mutant strain. Data are raw MIC values for each biological replicate in black with mean
683 MICs ± SEM in red. At least three biological replicates were performed. WH124: AB17978 with *lpxD*
684 insA *acfR* V136D *adeL* P131H ; C312*: Cysteine to stop codon at residue 312; Y324*: Tyrosine to
685 stop codon at residue 324. Statistical significance was tested using one-way ANOVA followed by
686 Dunnett's multiple comparison. Blue: multiple comparison against WT AB17978 MICs; Orange:
687 multiple comparison against MICs of Cy3a quadruple mutant. *: $p<0.05$; **: $p<0.01$; ****: $p<0.0001$;
688 ns: not significant.

689

690 **Figure 5. The LpxD E117K allele is tightly linked to clinical fluoroquinolone resistance**. A)
691 Assembled genomes of 139 clinical isolates with ciprofloxacin resistance profiles from PATRIC
692 database[80]. Displayed is heatmap showing the presence (orange; 1 isolate) or absence (white; 0
693 isolate) of clinical isolates for each ST type per each resistance group. B). LpxD sequences from
694 resistant (red dots) and susceptible isolates (green dots) were aligned and compared to ATCC
695 17978 and the total number of variants per residue was calculated for each group of genomes. The
696 total number of amino acid changes was normalized and presented as a *z*-score for each group,
697 plotted against the LpxD residue number. C). Hierarchical clustering of the 7-gene MLST profile
698 from 139 genes showing Euclidean distance as height and nodes color-coded with resistance profile
699 (red: CIP^R; blue: CIP^S) and the presence of LpxD E117K allele in purple. D). Structure of *Chlamydia*
700 *trachomatis* LpxD protein[38] showing the presumed site of the *A. baumannii* E117 based on sequence
701 similarity. E). Broth growth of AB17978 strains differing by single changes in *lpxD*. Shown are

702 strains harboring either the WT, *lpxD* T118A119_insA or *lpxD* E117K alleles. Statistical significance
703 was performed using one-way ANOVA followed by Dunnett's multiple comparison. ***: p-value <
704 0.001 for LpxD + A strain against WT. Data shown are mean ± SEM.

705

706 **Figure 6. The evolutionary trajectories of isolates acquired throughout passaging in**
707 **neutrophil-depleted mice is due to fitness advantage in presence of drug.** (A) A single *adeL*
708 mutant is outcompeted during infection of CIP-treated mice by a quadruple mutant (Cy31) having
709 drug resistant *adeLmfsA* alleles. The passage 9 pool was oropharyngeally inoculated into
710 neutrophil-depleted mice in duplicate but separate lineages and passaged three times in the
711 presence of CIP treatment, subjecting each passage to deep sequencing. A-B)Displayed are plots
712 showing relative abundance of all mutations identified in deep sequencing pools of the duplicate
713 passaging experiments as a function of the passage number) Competition of purified *adeL* and
714 quadruple mutant having *adeLmfsA* alleles in presence of CIP results in predominance of the
715 quadruple mutant. The two strains were mixed at a ratio 95:5 (single : quadruple mutant), and
716 oropharyngeally inoculated into neutrophil-depleted mice in the presence of CIP treatment through
717 three successive passages. Deep sequencing of the initial inoculum and each subsequent passage
718 was performed to determine the ratio of the two strains, and the relative abundance of each
719 mutation is displayed as a function of passage. C) The presence of neutrophils prevents enrichment
720 of an *adeL* mutant during CIP challenge in the mouse. Competition of designated mutants
721 (*adeL*ΔI335I336, *gyrA*S81L, or *gyrA*S81L *parC*S84L) against wild type AB17978 was performed. The
722 strains were mixed at a ratio 95 : 5 (AB17978 : mutant), oropharyngeally inoculated into
723 immunocompetent mice. and then passaged in duplicate but separate lineages three times in the
724 presence of CIP treatment. The abundance of each mutant was determined by measuring the colony
725 forming efficiency (CFE) at an antibiotic concentration that was below mutant MIC but above that

726 of wild type AB17978 (AdeL ΔI335I336 MIC: 0.75 μg/mL, GyrA S81L MIC: 0.75 μg/mL, or GyrA
727 S81L + ParC S84L MIC: 2 μg/mL), and the CFE versus passage number was displayed and expressed
728 as strain abundance (%). CFE = number of colonies on antibiotic-containing medium / number of
729 colonies in the absence of antibiotic.

730

731 **Figure 7. Simultaneous selection for increased resistance and fitness.** A) Growth rates in broth
732 culture of noted isolates from passages in mice. Significance determined by one-way ANOVA
733 followed by Dunnett's multiple comparison: **: $p<0.01$ for Cy11 against WT. C312*: mutation of
734 Cysteine to stop codon at residue 312. B) Neutrophil-replete and C) Neutrophil depleted
735 (cyclophosphamide treated) BALB/C mice were challenged oropharyngeally with noted strain
736 combinations for 24-hours to determine the selection rate for each competing pair of strains.
737 Selection rate coefficient (SRC) was determine by SRC = LN(Strain 1 output/input ratio) – LN(Strain
738 2 output/input ratio)(Materials and Methods) [72]. Data are mean ± SEM, with significance determine
739 by one-way ANOVA followed by B) Dunnett's or C) Tukey's Multiple Comparison. *$p<0.05$;
740 ****$p<0.0001$.

741

742 **Figure 8. Model of bacterial resistance progression.** The antibiotic susceptible inoculum (blue)
743 colonizes poorly in presence of antibiotic. During continued passage with CIP, in the absence of
744 neutrophils, the persister mutants (yellow) arise as first step mutations showing intermediate
745 MICs. With continued passage under the same antibiotic treatment regime, second step mutations
746 arise that have increased fitness in the presence of antibiotic (red) and dominate the population.

747

748 **Supplemental Figure 1. The LpxD E117K allele is tightly linked to clinical fluoroquinolone**
749 **resistance**. Assembled genomes of 2045 clinical isolates were obtained from PATRIC database[80].
750 LpxD sequences from all genomes were aligned and compared to ATCC 17978 and the total number
751 of variants per defined amino acid was calculated for each group of genomes. The total number of
752 amino acid changes was normalized and presented as a z-score for each of the three groups, plotted
753 against the residue numbers.

754

755 **Supplemental Figure 2. Distribution of MLST type among select clinical isolates.** A) Heatmap
756 showing MLST enrichment among 1830 genomes from ciprofloxacin resistant isolates and 269
757 genomes from susceptible isolates. In order to reduce the populational clonal effect, analysis was
758 limited to only one representative genome per ST group. Heatmap in B) shows the distribution of
759 MLST types after filtering.

760

761 **Supplemental Figure 3. Phylogenetic tree of genomes from 139 clinical isolates.** The genome
762 contigs were analyzed to build the phylogenetic tree using mashtree with the minimum abundance
763 finder.

764

765 **Supplemental Figure 4. Bacterial load and resistance levels to CIP after re-passaging.** A) The
766 bacterial load harvested from the lungs after each passage is plotted against the passage number for
767 each Lineage. B) CIP resistance level of each pool (after each passage) was assayed via
768 quantification of CFU on LB agar supplemented with CIP.

769

770 **Supp. Dataset 1**. MLST profiles with 7-gene allelic profiles for 2045 clinical isolates

771 **Supp. Dataset 2**. All mutations identified in Fig 2 with their detection frequency.

772 **Supp. Dataset 3**. Multiple alignment of LpxD sequences from 138 clinical isolates.

773 Competing Interests Statement

774 The authors declare that they have no conflict of interest.

775

776 Data availability statement.

777

778 Sequencing reads that support the findings of this study (Fig 2) are deposited in NCBI SRA with the
779 accession code PRJNA485355. Detailed accession numbers for each sample are listed in
780 Supplementary Table S1. Sequencing reads were analyzed by breseq
781 (https://github.com/barricklab/breseq) and all variants can be found at
782 https://github.com/huoww07/Ab_evolutionary_pathways. Variants were filtered against parent al
783 WT AB17978 and results are attached as Supp. Dataset 2. *A. baumannii* genome data used in this
784 study (Fig 5) are available in the PATRIC database (patricbrc.org) with the sequence IDs listed in
785 Supp. Dataset 1. All other data that support the findings of this study are available on request from
786 the corresponding author RRI.

787

788 # References

789 1 Boucher, H. W. *et al.* Bad Bugs, No Drugs: No ESKAPE! An Update from the Infectious
790 Diseases Society of America. *Clinical Infectious Diseases* **48**, 1-12, doi:10.1086/595011 (2009).

791 2 Valentine, S. C. *et al.* Phenotypic and Molecular Characterization of *Acinetobacter baumannii*
792 Clinical Isolates from Nosocomial Outbreaks in Los Angeles County, California. *Journal of Clinical*
793 *Microbiology* **46**, 2499-2507, doi:10.1128/jcm.00367-08 (2008).

794 3 Sievert, D. M. *et al.* Antimicrobial-Resistant Pathogens Associated with Healthcare-
795 Associated Infections Summary of Data Reported to the National Healthcare Safety Network at the
796 Centers for Disease Control and Prevention, 2009–2010. *Infection Control & Hospital Epidemiology*
797 **34**, 1-14, doi:10.1086/668770 (2015).

798 4 Karlowsky, J. A., Hoban, D. J., DeCorby, M. R., Laing, N. M. & Zhanel, G. G. Fluoroquinolone-
799 Resistant Urinary Isolates of *Escherichia coli* from Outpatients Are Frequently Multidrug Resistant:
800 Results from the North American Urinary Tract Infection Collaborative Alliance-Quinolone
801 Resistance Study. *Antimicrobial Agents and Chemotherapy* **50**, 2251-2254, doi:10.1128/aac.00123-
802 06 (2006).

803 5 Azim, A. *et al.* Epidemiology of bacterial colonization at intensive care unit admission with
804 emphasis on extended-spectrum β-lactamase- and metallo-β-lactamase-producing Gram-negative
805 bacteria – an Indian experience. *Journal of Medical Microbiology* **59**, 955-960,
806 doi:10.1099/jmm.0.018085-0 (2010).

807 6 Montefour, K. *et al. Acinetobacter baumannii:* an emerging multidrug-resistant pathogen in
808 critical care. *Crit Care Nurse* **28**, 15-25; quiz 26 (2008).

809 7 Zeighami, H., Valadkhani, F., Shapouri, R., Samadi, E. & Haghi, F. Virulence characteristics of
810 multidrug resistant biofilm forming *Acinetobacter baumannii* isolated from intensive care unit
811 patients. *BMC Infectious Diseases* **19**, doi:10.1186/s12879-019-4272-0 (2019).

812 8 Dijkshoorn, L., Nemec, A. & Seifert, H. An increasing threat in hospitals: multidrug-resistant
813 *Acinetobacter baumannii*. *Nature Reviews Microbiology* **5**, 939-951, doi:10.1038/nrmicro1789
814 (2007).

815 9 Ryan, K. *et al.* The impact of initial antibiotic treatment failure: Real-world insights in
816 healthcare-associated or nosocomial pneumonia. *Journal of Infection* **77**, 9-17,
817 doi:10.1016/j.jinf.2018.04.002 (2018).

818 10 Wong, D. *et al.* Clinical and Pathophysiological Overview of *Acinetobacter* Infections: a
819 Century of Challenges. *Clin Microbiol Rev* **30**, 409-447, doi:10.1128/CMR.00058-16 (2017).

820 11 Fernandez-Cuenca, F. Relationship between beta-lactamase production, outer membrane
821 protein and penicillin-binding protein profiles on the activity of carbapenems against clinical
822 isolates of *Acinetobacter baumannii*. *Journal of Antimicrobial Chemotherapy* **51**, 565-574,
823 doi:10.1093/jac/dkg097 (2003).

824 12 Lolans, K., Rice, T. W., Munoz-Price, L. S. & Quinn, J. P. Multicity outbreak of carbapenem-
825 resistant *Acinetobacter baumannii* isolates producing the carbapenemase OXA-40. *Antimicrob*
826 *Agents Chemother* **50**, 2941-2945, doi:10.1128/AAC.00116-06 (2006).

827 13 Geisinger, E. & Isberg, R. R. Antibiotic modulation of capsular exopolysaccharide and
828 virulence in *Acinetobacter baumannii*. *PLoS Pathog* **11**, e1004691,
829 doi:10.1371/journal.ppat.1004691 (2015).

830 14 Aldred, K. J., Kerns, R. J. & Osheroff, N. Mechanism of quinolone action and resistance.
831 *Biochemistry* **53**, 1565-1574, doi:10.1021/bi5000564 (2014).

832 15 Redgrave, L. S., Sutton, S. B., Webber, M. A. & Piddock, L. J. V. Fluoroquinolone resistance:
833 mechanisms, impact on bacteria, and role in evolutionary success. *Trends in Microbiology* **22**, 438-
834 445, doi:10.1016/j.tim.2014.04.007 (2014).

835 16 Hujer, K. M. *et al.* Rapid Determination of Quinolone Resistance in *Acinetobacter spp*. *Journal*
836 *of Clinical Microbiology* **47**, 1436-1442, doi:10.1128/jcm.02380-08 (2009).

837 17 Munoz-Price, L. S. & Weinstein, R. A. Acinetobacter infection. *N Engl J Med* **358**, 1271-1281,
838 doi:10.1056/NEJMra070741 (2008).

839 18 Ankomah, P. & Levin, B. R. Exploring the collaboration between antibiotics and the immune
840 response in the treatment of acute, self-limiting infections. *Proc Natl Acad Sci U S A* **111**, 8331-8338,
841 doi:10.1073/pnas.1400352111 (2014).

842 19 Wheatley, R. *et al.* Rapid evolution and host immunity drive the rise and fall of carbapenem
843 resistance during an acute *Pseudomonas aeruginosa* infection. *Nat Commun* **12**, 2460,
844 doi:10.1038/s41467-021-22814-9 (2021).

845 20 Saroj, S. D., Clemmer, K. M., Bonomo, R. A. & Rather, P. N. Novel Mechanism for
846 Fluoroquinolone Resistance in *Acinetobacter baumannii*. *Antimicrobial Agents and Chemotherapy*
847 **56**, 4955-4957, doi:10.1128/aac.00739-12 (2012).

848 21 Osińska, A., Harnisz, M. & Korzeniewska, E. Prevalence of plasmid-mediated multidrug
849 resistance determinants in fluoroquinolone-resistant bacteria isolated from sewage and surface
850 water. *Environmental Science and Pollution Research* **23**, 10818-10831, doi:10.1007/s11356-016-
851 6221-4 (2016).

852 22 Elhosseiny, N. M., Elhezawy, N. B. & Attia, A. S. Comparative proteomics analyses of
853 *Acinetobacter baumannii* strains ATCC 17978 and AB5075 reveal the differential role of type II

854 secretion system secretomes in lung colonization and ciprofloxacin resistance. *Microbial*
855 *Pathogenesis* **128**, 20-27, doi:10.1016/j.micpath.2018.12.039 (2019).

856 23 Zuluaga, A. F. *et al.* Neutropenia induced in outbred mice by a simplified low-dose
857 cyclophosphamide regimen: characterization and applicability to diverse experimental models of
858 infectious diseases. *BMC Infect Dis* **6**, 55, doi:10.1186/1471-2334-6-55 (2006).

859 24 North, R. J. Cyclophosphamide-facilitated adoptive immunotherapy of an established tumor
860 depends on elimination of tumor-induced suppressor T cells. *J Exp Med* **155**, 1063-1074,
861 doi:10.1084/jem.155.4.1063 (1982).

862 25 Yoon, E. J. *et al.* Contribution of resistance-nodulation-cell division efflux systems to
863 antibiotic resistance and biofilm formation in *Acinetobacter baumannii*. *mBio* **6**,
864 doi:10.1128/mBio.00309-15 (2015).

865 26 Coyne, S., Rosenfeld, N., Lambert, T., Courvalin, P. & Perichon, B. Overexpression of
866 resistance-nodulation-cell division pump AdeFGH confers multidrug resistance in *Acinetobacter*
867 *baumannii*. *Antimicrob Agents Chemother* **54**, 4389-4393, doi:10.1128/AAC.00155-10 (2010).

868 27 USCAST. The United States Committee on Antimicrobial Susceptibility Testing (USCAST).
869 Breakpoint tables for interpretation of MIC and zone diameter results. Version 6.0. (2020).

870 28 Brauner, A., Fridman, O., Gefen, O. & Balaban, N. Q. Distinguishing between resistance,
871 tolerance and persistence to antibiotic treatment. *Nat Rev Microbiol* **14**, 320-330,
872 doi:10.1038/nrmicro.2016.34 (2016).

873 29 Kussell, E., Kishony, R., Balaban, N. Q. & Leibler, S. Bacterial persistence: a model of survival
874 in changing environments. *Genetics* **169**, 1807-1814, doi:10.1534/genetics.104.035352 (2005).

875 30 Balaban, N. Q. Persistence: mechanisms for triggering and enhancing phenotypic variability.
876 *Curr Opin Genet Dev* **21**, 768-775, doi:10.1016/j.gde.2011.10.001 (2011).

877 31 Balaban, N. Q. *et al.* Definitions and guidelines for research on antibiotic persistence. *Nat Rev*
878 *Microbiol* **17**, 441-448, doi:10.1038/s41579-019-0196-3 (2019).

879 32 Liu, J., Gefen, O., Ronin, I., Bar-Meir, M. & Balaban, N. Q. Effect of tolerance on the evolution of
880 antibiotic resistance under drug combinations. *Science* **367**, 200-204, doi:10.1126/science.aay3041
881 (2020).

882 33 Papkou, A., Hedge, J., Kapel, N., Young, B. & MacLean, R. C. Efflux pump activity potentiates
883 the evolution of antibiotic resistance across *S. aureus* isolates. *Nat Commun* **11**, 3970,
884 doi:10.1038/s41467-020-17735-y (2020).

885 34 Santos-Lopez, A., Marshall, C. W., Scribner, M. R., Snyder, D. J. & Cooper, V. S. Evolutionary
886 pathways to antibiotic resistance are dependent upon environmental structure and bacterial
887 lifestyle. *eLife* **8**, doi:10.7554/eLife.47612 (2019).

888 35 Raetz, C. R. H., Reynolds, C. M., Trent, M. S. & Bishop, R. E. Lipid A Modification Systems in
889 Gram-Negative Bacteria. *Annual Review of Biochemistry* **76**, 295-329,
890 doi:10.1146/annurev.biochem.76.010307.145803 (2007).

891 36 Lathe, R. & Lecocq, J. P. The firA gene, a locus involved in the expression of rifampicin
892 resistance in *Escherichia coli*. *Molecular and General Genetics MGG* **154**, 53-60,
893 doi:10.1007/bf00265576 (1977).

894 37 Kelly, T. M., Stachula, S. A., Raetz, C. R. & Anderson, M. S. The firA gene of *Escherichia coli*
895 encodes UDP-3-O-(R-3-hydroxymyristoyl)-glucosamine N-acyltransferase. The third step of
896 endotoxin biosynthesis. *J Biol Chem* **268**, 19866-19874 (1993).

897 38 Buetow, L., Smith, T. K., Dawson, A., Fyffe, S. & Hunter, W. N. Structure and reactivity of
898 LpxD, the N-acyltransferase of lipid A biosynthesis. *Proceedings of the National Academy of Sciences*
899 **104**, 4321-4326, doi:10.1073/pnas.0606356104 (2007).

900 39 Jolley, K. A., Bray, J. E. & Maiden, M. C. J. Open-access bacterial population genomics: BIGSdb
901 software, the PubMLST.org website and their applications. *Wellcome Open Res* **3**, 124,
902 doi:10.12688/wellcomeopenres.14826.1 (2018).

903 40 Blount, Z. D., Lenski, R. E. & Losos, J. B. Contingency and determinism in evolution:
904 Replaying life's tape. *Science* **362**, doi:10.1126/science.aam5979 (2018).

905 41 Melnyk, A. H., Wong, A. & Kassen, R. The fitness costs of antibiotic resistance mutations.
906 *Evolutionary Applications* **8**, 273-283, doi:10.1111/eva.12196 (2014).

907 42 Subedi, D., Vijay, A. K., Kohli, G. S., Rice, S. A. & Willcox, M. Comparative genomics of clinical
908 strains of *Pseudomonas aeruginosa* strains isolated from different geographic sites. *Scientific*
909 *Reports* **8**, doi:10.1038/s41598-018-34020-7 (2018).

910 43 Lieberman, T. D. *et al.* Genetic variation of a bacterial pathogen within individuals with
911 cystic fibrosis provides a record of selective pressures. *Nature Genetics* **46**, 82-87,
912 doi:10.1038/ng.2848 (2013).

913 44 Lieberman, T. D. *et al.* Parallel bacterial evolution within multiple patients identifies
914 candidate pathogenicity genes. *Nature Genetics* **43**, 1275-1280, doi:10.1038/ng.997 (2011).

915 45 Choi, B. *et al.* Persistence and Evolution of SARS-CoV-2 in an Immunocompromised Host.
916 *New England Journal of Medicine* **383**, 2291-2293, doi:10.1056/NEJMc2031364 (2020).

917 46 Honsa, E. S. *et al.* RelA Mutant *Enterococcus faecium* with Multiantibiotic Tolerance Arising
918 in an Immunocompromised Host. *mBio* **8**, doi:10.1128/mBio.02124-16 (2017).

919 47 Ma, C., Yang, X. & Lewis, P. J. Bacterial Transcription as a Target for Antibacterial Drug
920 Development. *Microbiology and Molecular Biology Reviews* **80**, 139-160, doi:10.1128/mmbr.00055-
921 15 (2016).

922 48 van Hoek, A. H. A. M. *et al.* Acquired Antibiotic Resistance Genes: An Overview. *Frontiers in*
923 *Microbiology* **2**, doi:10.3389/fmicb.2011.00203 (2011).

924 49 Moyed, H. S. & Bertrand, K. P. hipA, a newly recognized gene of *Escherichia coli* K-12 that
925 affects frequency of persistence after inhibition of murein synthesis. *J Bacteriol* **155**, 768-775,
926 doi:10.1128/JB.155.2.768-775.1983 (1983).

927 50 Schumacher, M. A. *et al.* HipBA-promoter structures reveal the basis of heritable multidrug
928 tolerance. *Nature* **524**, 59-64, doi:10.1038/nature14662 (2015).

929 51 Pontes, M. H., Groisman, E. A. & Garsin, D. A. A Physiological Basis for Nonheritable
930 Antibiotic Resistance. *mBio* **11**, doi:10.1128/mBio.00817-20 (2020).

931 52 Trastoy, R. *et al.* Mechanisms of Bacterial Tolerance and Persistence in the Gastrointestinal
932 and Respiratory Environments. *Clinical Microbiology Reviews* **31**, doi:10.1128/cmr.00023-18
933 (2018).

934 53 Balaban, N. Q., Merrin, J., Chait, R., Kowalik, L. & Leibler, S. Bacterial persistence as a
935 phenotypic switch. *Science* **305**, 1622-1625, doi:10.1126/science.1099390 (2004).

936 54 Lewis, K. Persister cells, dormancy and infectious disease. *Nat Rev Microbiol* **5**, 48-56,
937 doi:10.1038/nrmicro1557 (2007).

938 55 Shah, D. *et al.* Persisters: a distinct physiological state of E. coli. *BMC Microbiol* **6**, 53,
939 doi:10.1186/1471-2180-6-53 (2006).

940 56 Nandakumar, M., Nathan, C. & Rhee, K. Y. Isocitrate lyase mediates broad antibiotic
941 tolerance in *Mycobacterium tuberculosis*. *Nature Communications* **5**, doi:10.1038/ncomms5306
942 (2014).

943 57 Michiels, J. E., Van den Bergh, B., Verstraeten, N. & Michiels, J. Molecular mechanisms and
944 clinical implications of bacterial persistence. *Drug Resistance Updates* **29**, 76-89,
945 doi:10.1016/j.drup.2016.10.002 (2016).

946 58 Fisher, R. A., Gollan, B. & Helaine, S. Persistent bacterial infections and persister cells. *Nature*
947 *Reviews Microbiology* **15**, 453-464, doi:10.1038/nrmicro.2017.42 (2017).

948 59 Van den Bergh, B., Fauvart, M. & Michiels, J. Formation, physiology, ecology, evolution and
949 clinical importance of bacterial persisters. *FEMS Microbiology Reviews* **41**, 219-251,
950 doi:10.1093/femsre/fux001 (2017).

951 60 Yoon, E. J., Courvalin, P. & Grillot-Courvalin, C. RND-type efflux pumps in multidrug-resistant
952 clinical isolates of *Acinetobacter baumannii*: major role for AdeABC overexpression and AdeRS
953 mutations. *Antimicrob Agents Chemother* **57**, 2989-2995, doi:10.1128/AAC.02556-12 (2013).

954 61 Pu, Y. *et al.* Enhanced Efflux Activity Facilitates Drug Tolerance in Dormant Bacterial Cells.
955 *Molecular Cell* **62**, 284-294, doi:10.1016/j.molcel.2016.03.035 (2016).

956 62 Harms, A., Maisonneuve, E. & Gerdes, K. Mechanisms of bacterial persistence during stress
957 and antibiotic exposure. *Science* **354**, doi:10.1126/science.aaf4268 (2016).

958 63 Frimodt-Møller, J. & Løbner-Olesen, A. Efflux-Pump Upregulation: From Tolerance to High-
959 level Antibiotic Resistance? *Trends in Microbiology* **27**, 291-293, doi:10.1016/j.tim.2019.01.005
960 (2019).

961 64 El Meouche, I. & Dunlop, M. J. Heterogeneity in efflux pump expression predisposes
962 antibiotic-resistant cells to mutation. *Science* **362**, 686-690, doi:10.1126/science.aar7981 (2018).

963 65 Nolivos, S. *et al.* Role of AcrAB-TolC multidrug efflux pump in drug-resistance acquisition by
964 plasmid transfer. *Science* **364**, 778-782, doi:10.1126/science.aav6390 (2019).

965 66 Peeters, P. *et al.* The impact of initial antibiotic treatment failure: real-world insights in
966 patients with complicated, health care-associated intra-abdominal infection. *Infection and Drug*
967 *Resistance* **Volume 12**, 329-343, doi:10.2147/idr.S184116 (2019).

968 67 Soriano, A., Mensa, J., Meylan, S., Morata, L. & Kuehl, R. When antibiotics fail: a clinical and
969 microbiological perspective on antibiotic tolerance and persistence of *Staphylococcus aureus*.
970 *Journal of Antimicrobial Chemotherapy* **75**, 1071-1086, doi:10.1093/jac/dkz559 (2020).

971 68 Meylan, S., Andrews, I. W. & Collins, J. J. Targeting Antibiotic Tolerance, Pathogen by
972 Pathogen. *Cell* **172**, 1228-1238, doi:10.1016/j.cell.2018.01.037 (2018).

973 69 Karve, S. *et al.* The impact of initial antibiotic treatment failure: Real-world insights in
974 patients with complicated urinary tract infection. *Journal of Infection* **76**, 121-131,
975 doi:10.1016/j.jinf.2017.11.001 (2018).

976 70 Wang, E. *et al.* Pathogenesis of Pneumococcal Pneumonia in Cyclophosphamide-Induced
977 Leukopenia in Mice. *Infection and Immunity* **70**, 4226-4238, doi:10.1128/iai.70.8.4226-4238.2002
978 (2002).

979 71 Nielsen, T. B., Yan, J., Luna, B. & Spellberg, B. Murine Oropharyngeal Aspiration Model of
980 Ventilator-associated and Hospital-acquired Bacterial Pneumonia. *Journal of Visualized*
981 *Experiments*, doi:10.3791/57672 (2018).

982 72 Travisano, M. & Lenski, R. E. Long-term experimental evolution in *Escherichia coli*. IV.
983 Targets of selection and the specificity of adaptation. *Genetics* **143**, 15-26,
984 doi:10.1093/genetics/143.1.15 (1996).

985 73 Geisinger, E., Mortman, N. J., Vargas-Cuebas, G., Tai, A. K. & Isberg, R. R. A global regulatory
986 system links virulence and antibiotic resistance to envelope homeostasis in *Acinetobacter*
987 *baumannii*. *PLoS Pathog* **14**, e1007030, doi:10.1371/journal.ppat.1007030 (2018).

988 74 Deatherage, D. E. & Barrick, J. E. Identification of mutations in laboratory-evolved microbes
989 from next-generation sequencing data using breseq. *Methods Mol Biol* **1151**, 165-188,
990 doi:10.1007/978-1-4939-0554-6_12 (2014).

991 75 Wijers, C. D. M. *et al.* Identification of Two Variants of *Acinetobacter baumannii* Strain ATCC
992 17978 with Distinct Genotypes and Phenotypes. *Infect Immun* **89**, e0045421,
993 doi:10.1128/IAI.00454-21 (2021).

994 76 Choi, Y., Sims, G. E., Murphy, S., Miller, J. R. & Chan, A. P. Predicting the functional effect of
995 amino acid substitutions and indels. *PLoS One* **7**, e46688, doi:10.1371/journal.pone.0046688
996 (2012).

997 77 Yanisch-Perron, C., Vieira, J. & Messing, J. Improved M13 phage cloning vectors and host
998 strains: nucleotide sequences of the M13mpl8 and pUC19 vectors. *Gene* **33**, 103-119,
999 doi:10.1016/0378-1119(85)90120-9 (1985).

1000 78 Andrews, H. L., Vogel, J. P. & Isberg, R. R. Identification of linked *Legionella pneumophila*
1001 genes essential for intracellular growth and evasion of the endocytic pathway. *Infect Immun* **66**,
1002 950-958, doi:10.1128/IAI.66.3.950-958.1998 (1998).

1003 79 Katz, L. S. *et al.* Mashtree: a rapid comparison of whole genome sequence files. *Journal of*
1004 *Open Source Software* **4**, doi: 10.21105/joss.01762 (2019).

1005 80 Davis, J. J. *et al.* The PATRIC Bioinformatics Resource Center: expanding data and analysis
1006 capabilities. *Nucleic Acids Research*, doi:10.1093/nar/gkz943 (2019).

1007

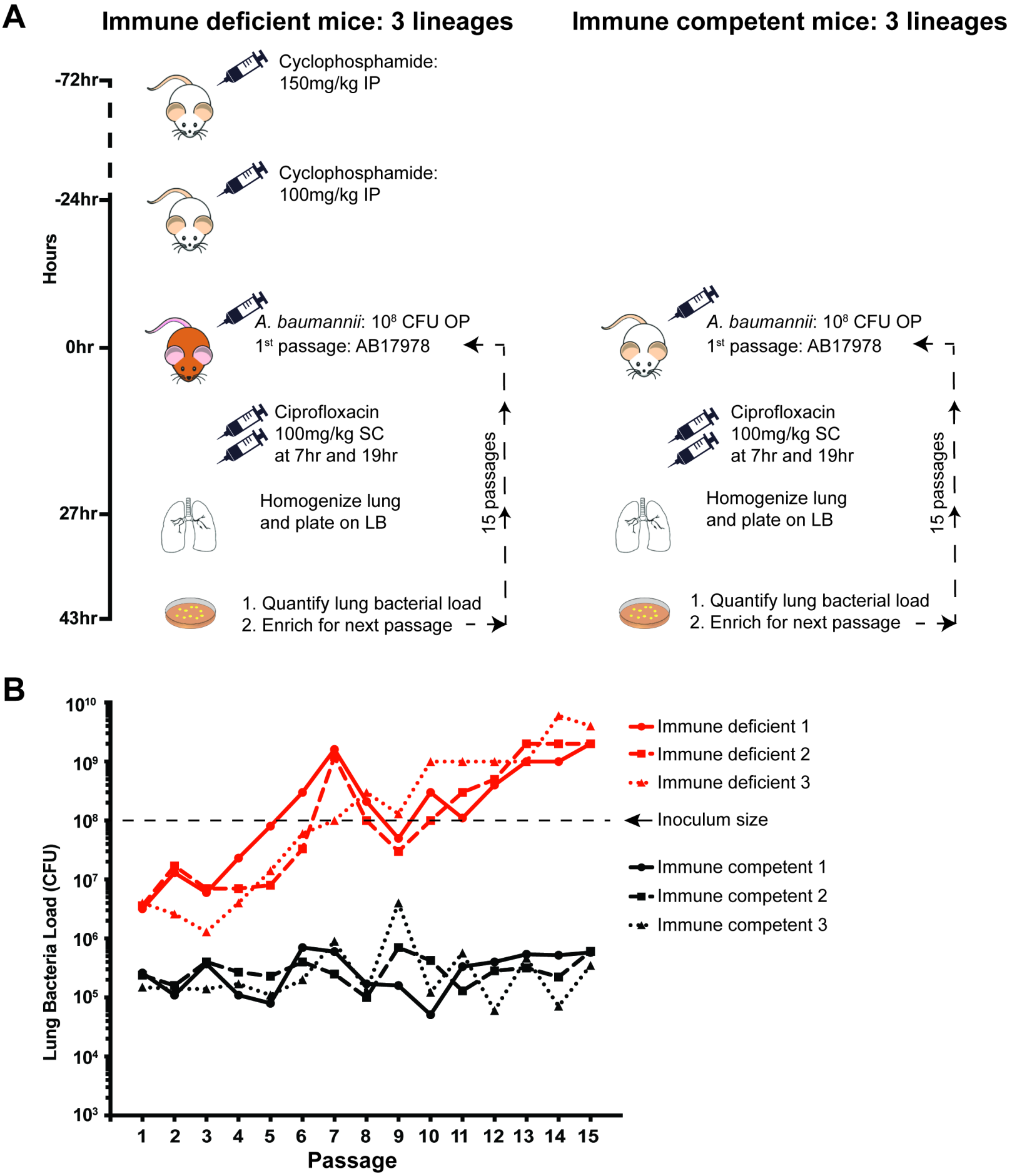
A
Immune deficient mice: 3 lineages
Immune competent mice: 3 lineages
-72hr
Cyclophosphamide:
150mg/kg IP
-24hr
Cyclophosphamide:
100mg/kg IP
Hours
0hr
A. baumannii: 10⁸ CFU OP
1st passage: AB17978
Ciprofloxacin
100mg/kg SC
at 7hr and 19hr
27hr
Homogenize lung
and plate on LB
15 passages
43hr
1. Quantify lung bacterial load
2. Enrich for next passage
B
Lung Bacteria Load (CFU)
10¹⁰
10⁹
10⁸
10⁷
10⁶
10⁵
10⁴
10³
1 2 3 4 5 6 7 8 9 10 11 12 13 14 15
Passage
Immune deficient 1
Immune deficient 2
Immune deficient 3
Inoculum size
Immune competent 1
Immune competent 2
Immune competent 3

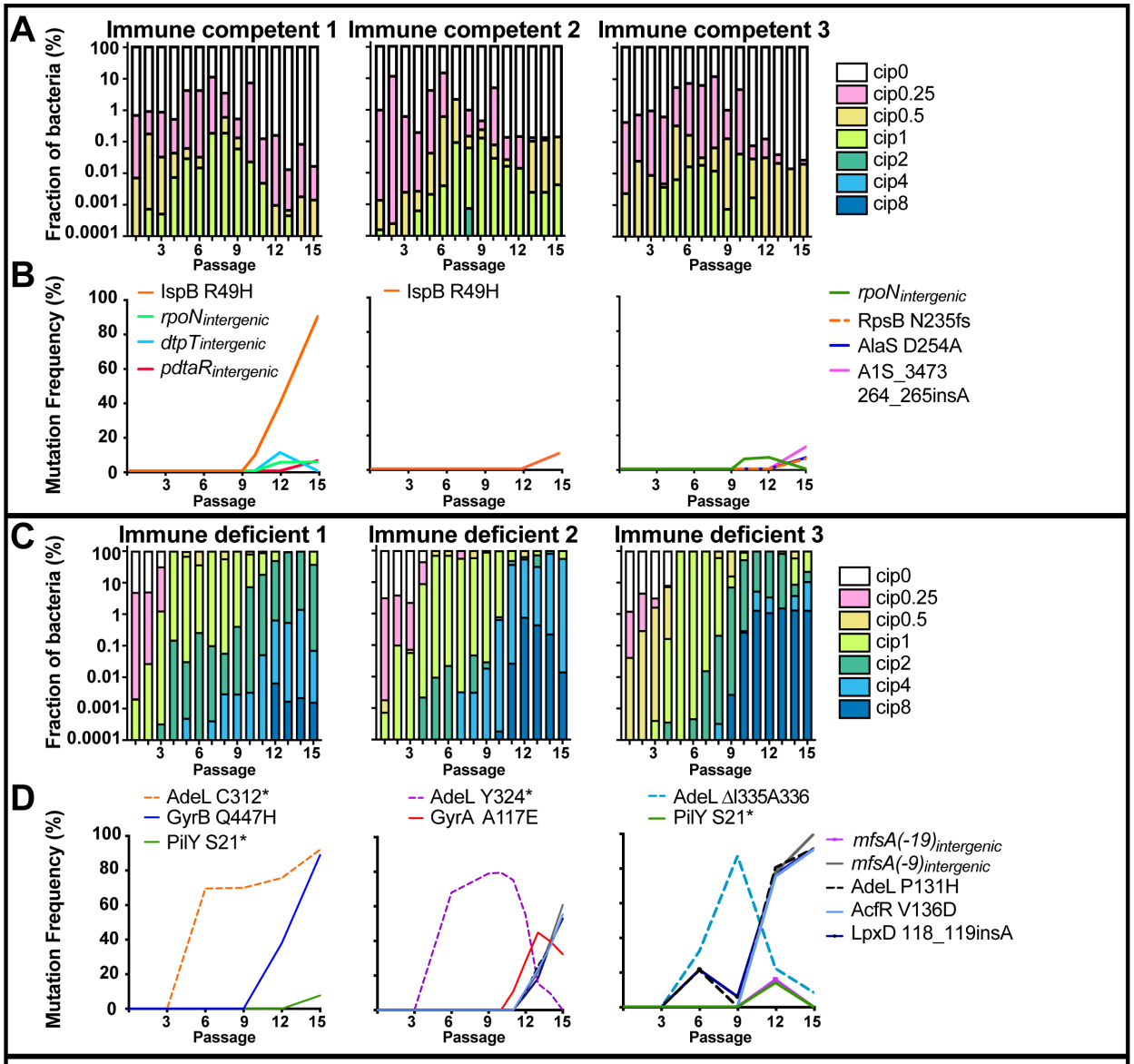
A
Immune competent 1
Immune competent 2
Immune competent 3
Fraction of bacteria (%)
Passage
cip0
cip0.25
cip0.5
cip1
cip2
cip4
cip8
B
Mutation Frequency (%)
IspB R49H
rpoN intergenic
dtpT intergenic
pdtaR intergenic
RpsB N235fs
AlaS D254A
A1S_3473 264_265insA
C
Immune deficient 1
Immune deficient 2
Immune deficient 3
D
AdeL C312*
GyrB Q447H
PilY S21*
AdeL Y324*
GyrA A117E
AdeL ΔI335A336
mfsA(-19) intergenic
mfsA(-9) intergenic
AdeL P131H
AcfR V136D
LpxD 118_119insA

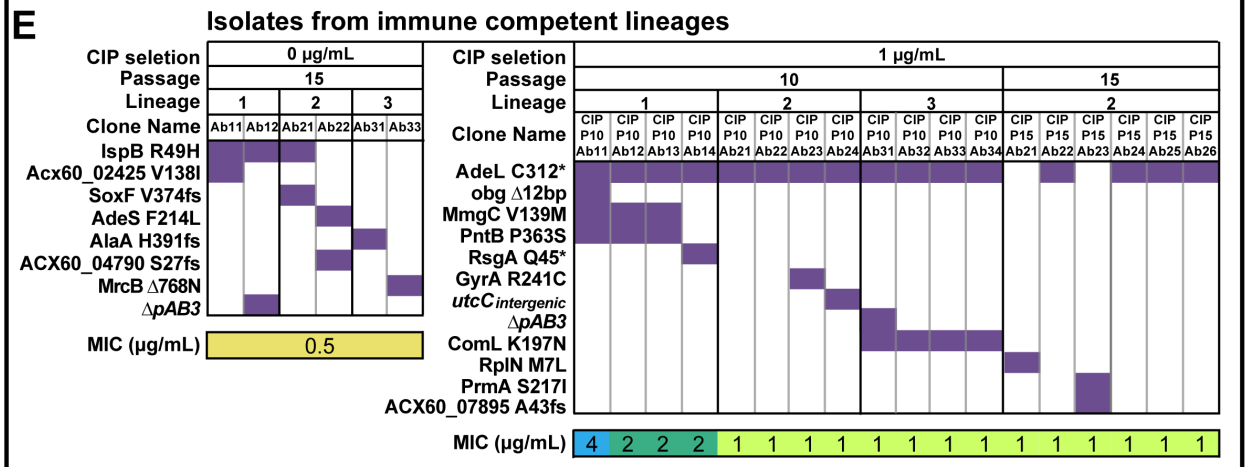
E
Isolates from immune competent lineages
CIP seletion
Passage
Lineage
Clone Name
IspB R49H
Acx60_02425 V138I
SoxF V374fs
AdeS F214L
AlaA H391fs
ACX60_04790 S27fs
MrcB Δ768N
ΔpAB3
MIC (μg/mL)
0 μg/mL
1 μg/mL
AdeL C312*
obg Δ12bp
MmgC V139M
PntB P363S
RsgA Q45*
GyrA R241C
utcC intergenic
ΔpAB3
ComL K197N
RplN M7L
PrmA S217I
ACX60_07895 A43fs

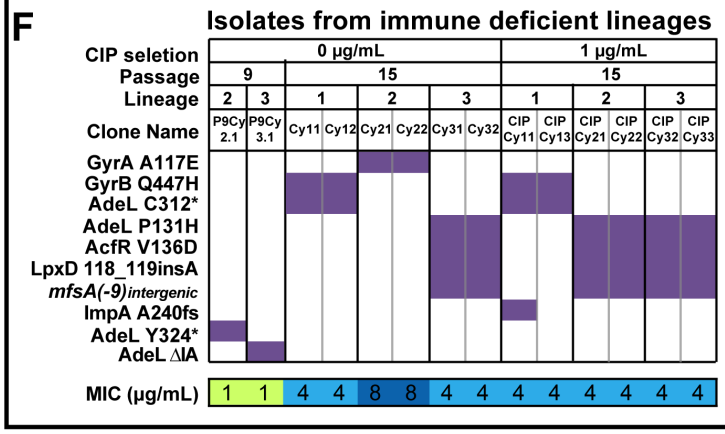
F
Isolates from immune deficient lineages
CIP seletion
Passage
Lineage
Clone Name
GyrA A117E
GyrB Q447H
AdeL C312*
AdeL P131H
AcfR V136D
LpxD 118_119insA
mfsA(-9) intergenic
ImpA A240fs
AdeL Y324*
AdeL ΔIA
MIC (μg/mL)
0 μg/mL
1 μg/mL

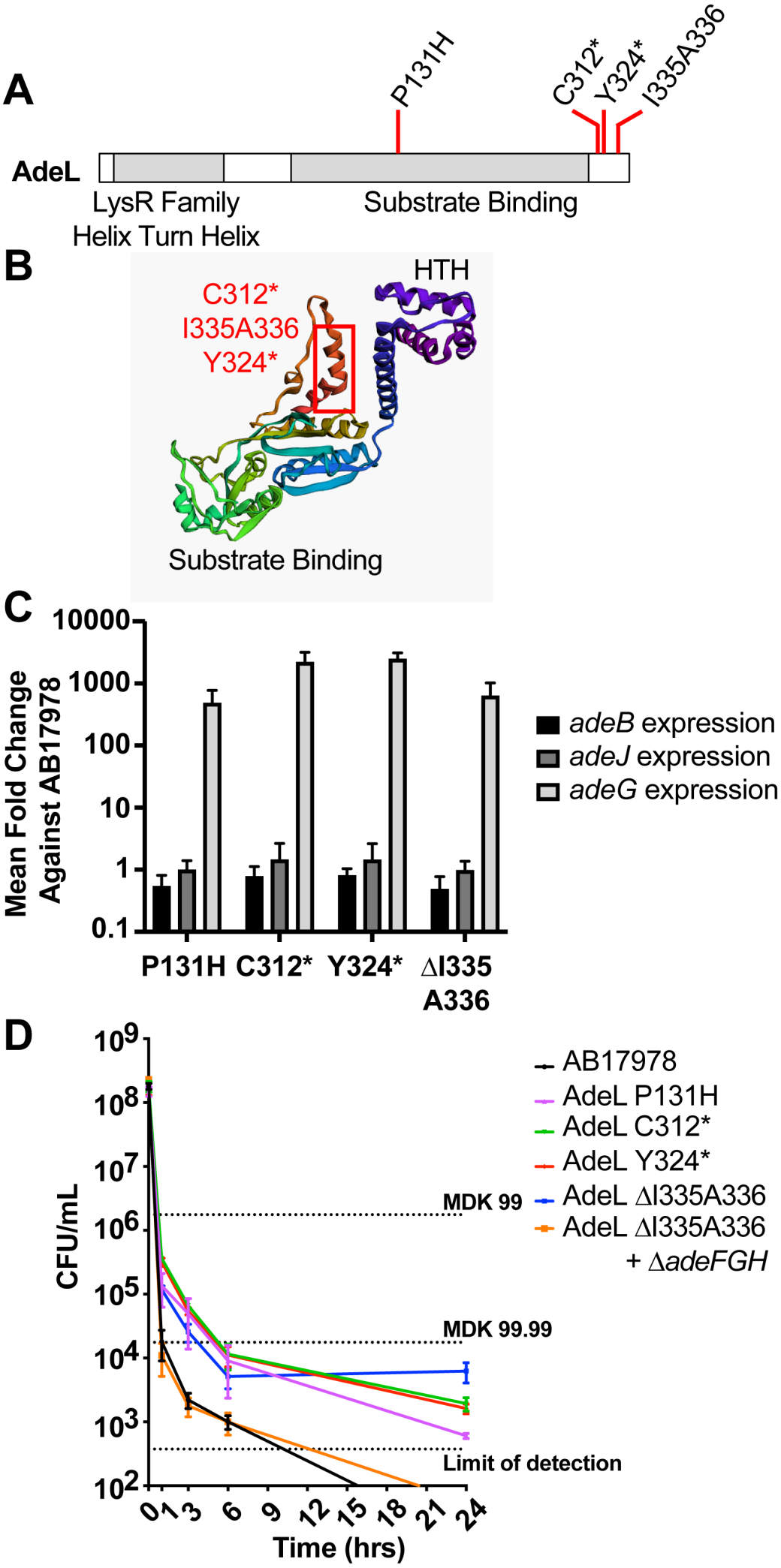
A
P131H
C312*
Y324*
I335A336
AdeL
LysR Family
Helix Turn Helix
Substrate Binding
B
HTH
C312*
I335A336
Y324*
Substrate Binding
C
Mean Fold Change Against AB17978
10000
1000
100
10
1
0.1
P131H
C312*
Y324*
ΔI335 A336
adeB expression
adeJ expression
adeG expression
D
CFU/mL
10^9
10^8
10^7
10^6
10^5
10^4
10^3
10^2
MDK 99
MDK 99.99
Limit of detection
0 1 3 6 9 12 15 18 21 24
Time (hrs)
AB17978
AdeL P131H
AdeL C312*
AdeL Y324*
AdeL ΔI335A336
AdeL ΔI335A336 + ΔadeFGH

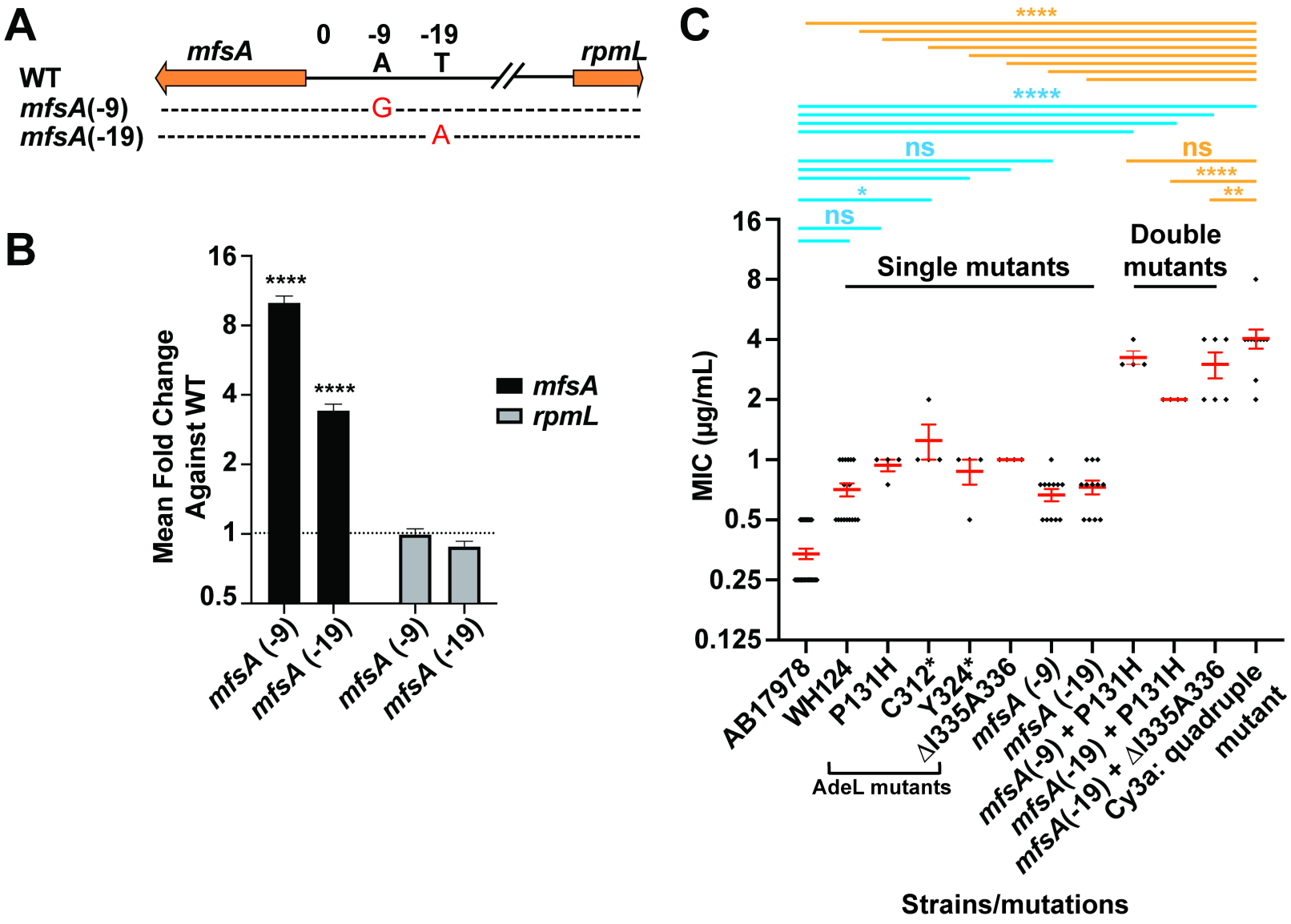
A
mfsA
0
-9
A
-19
T
rpmL
WT
mfsA(-9)
G
mfsA(-19)
A
B
Mean Fold Change Against WT
16
8
4
2
1
0.5
****
****
mfsA
rpmL
mfsA (-9)
mfsA (-19)
mfsA (-9)
mfsA (-19)
C
****
****
ns
ns
*
ns
****
**
Single mutants
Double mutants
MIC (µg/mL)
16
8
4
2
1
0.5
0.25
0.125
AB17978
WH124
P131H
C312*
Y324*
ΔI335A336
mfsA (-9)
mfsA (-19)
mfsA(-9) + P131H
mfsA(-19) + P131H
mfsA(-19) + ΔI335A336
Cy3a: quadruple mutant
AdeL mutants
Strains/mutations

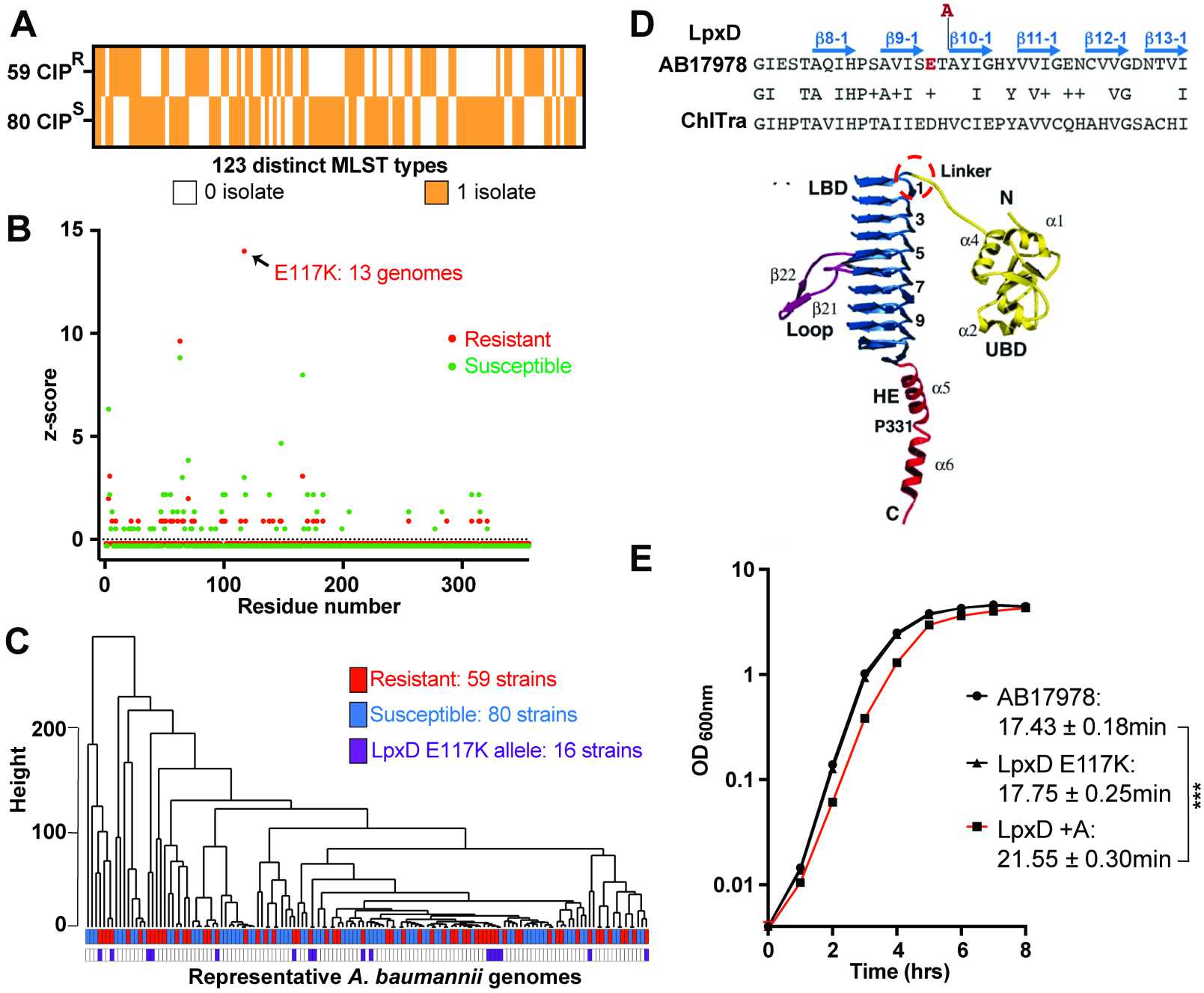
A
59 CIP^R
80 CIP^S
123 distinct MLST types
0 isolate
1 isolate
B
E117K: 13 genomes
Resistant
Susceptible
z-score
Residue number
C
Resistant: 59 strains
Susceptible: 80 strains
LpxD E117K allele: 16 strains
Height
Representative A. baumannii genomes
D
LpxD
AB17978 GIESTAQIHPSAVISETAYIGHYVVIGENCVVGDNTVI
ChlTra GIHPTAVIHPTAIIEDHVCIEPYAVVCQHAHVGSACHI
β8-1
β9-1
β10-1
β11-1
β12-1
β13-1
A
LBD
Linker
N
α1
α4
β22
β21
Loop
α2
UBD
HE
α5
P331
α6
C
E
OD 600nm
Time (hrs)
AB17978:
17.43 ± 0.18min
LpxD E117K:
17.75 ± 0.25min
LpxD +A:
21.55 ± 0.30min
***

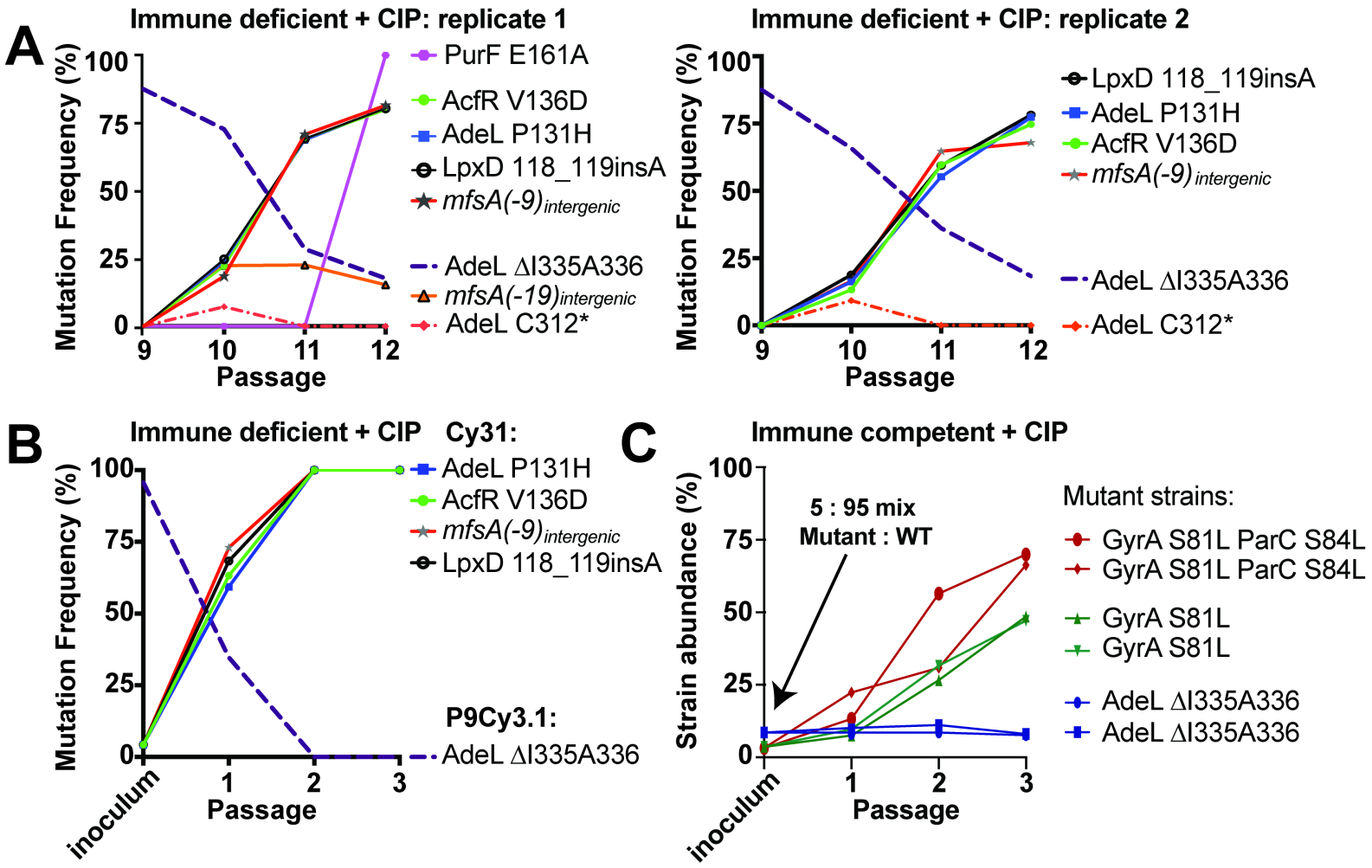
A
Immune deficient + CIP: replicate 1
Mutation Frequency (%)
100
75
50
25
0
9
10
11
12
Passage
PurF E161A
AcfR V136D
AdeL P131H
LpxD 118_119insA
mfsA(-9)intergenic
AdeL ΔI335A336
mfsA(-19)intergenic
AdeL C312*
Immune deficient + CIP: replicate 2
Mutation Frequency (%)
100
75
50
25
0
9
10
11
12
Passage
LpxD 118_119insA
AdeL P131H
AcfR V136D
mfsA(-9)intergenic
AdeL ΔI335A336
AdeL C312*
B
Immune deficient + CIP
Cy31:
Mutation Frequency (%)
100
75
50
25
0
inoculum
1
2
3
Passage
AdeL P131H
AcfR V136D
mfsA(-9)intergenic
LpxD 118_119insA
P9Cy3.1:
AdeL ΔI335A336
C
Immune competent + CIP
Strain abundance (%)
100
75
50
25
0
5 : 95 mix
Mutant : WT
inoculum
1
2
3
Passage
Mutant strains:
GyrA S81L ParC S84L
GyrA S81L ParC S84L
GyrA S81L
GyrA S81L
AdeL ΔI335A336
AdeL ΔI335A336

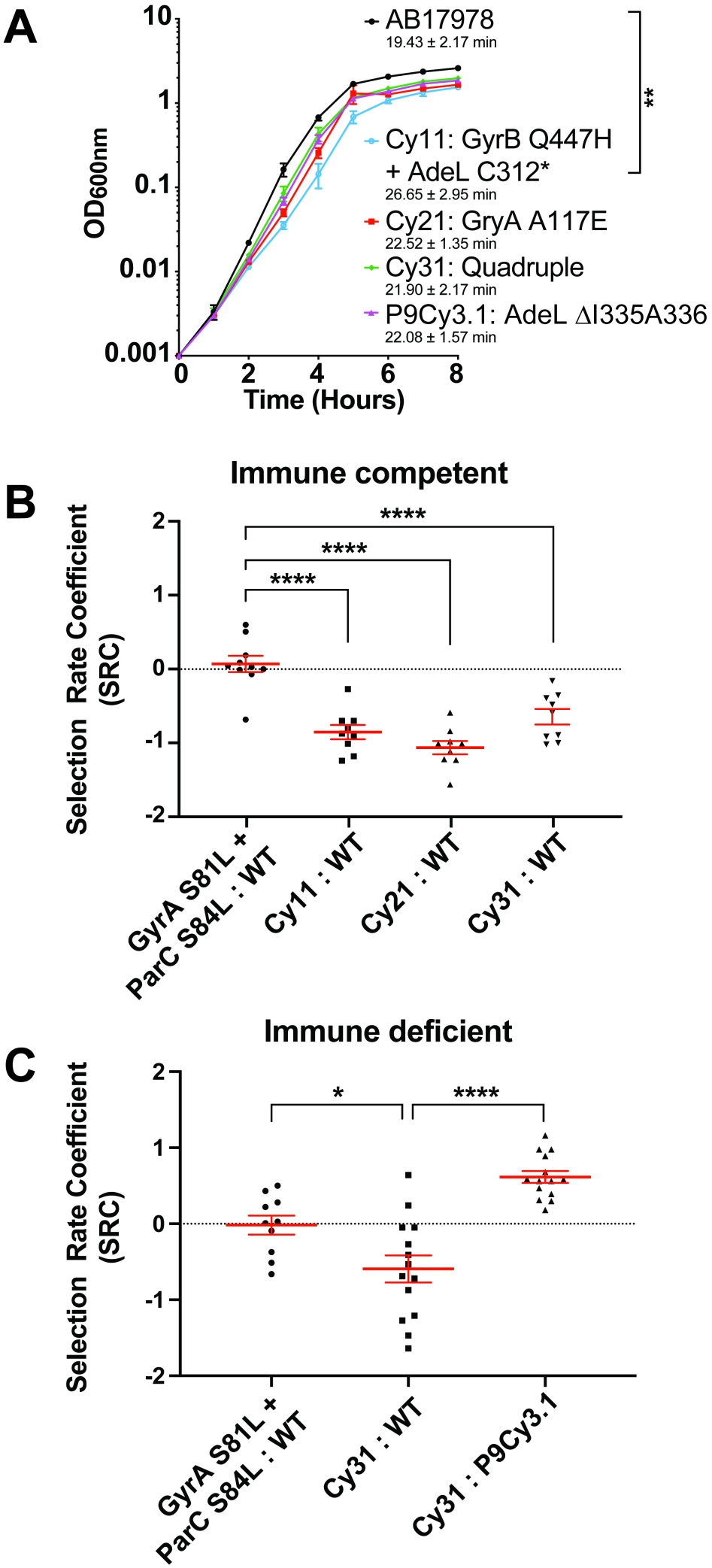
A
AB17978
19.43 ± 2.17 min
Cy11: GyrB Q447H
+ AdeL C312*
26.65 ± 2.95 min
Cy21: GryA A117E
22.52 ± 1.35 min
Cy31: Quadruple
21.90 ± 2.17 min
P9Cy3.1: AdeL ΔI335A336
22.08 ± 1.57 min
**
OD600nm
Time (Hours)
B
Immune competent
Selection Rate Coefficient (SRC)
****
****
****
GyrA S81L + ParC S84L : WT
Cy11 : WT
Cy21 : WT
Cy31 : WT
C
Immune deficient
Selection Rate Coefficient (SRC)
*
****
GyrA S81L + ParC S84L : WT
Cy31 : WT
Cy31 : P9Cy3.1

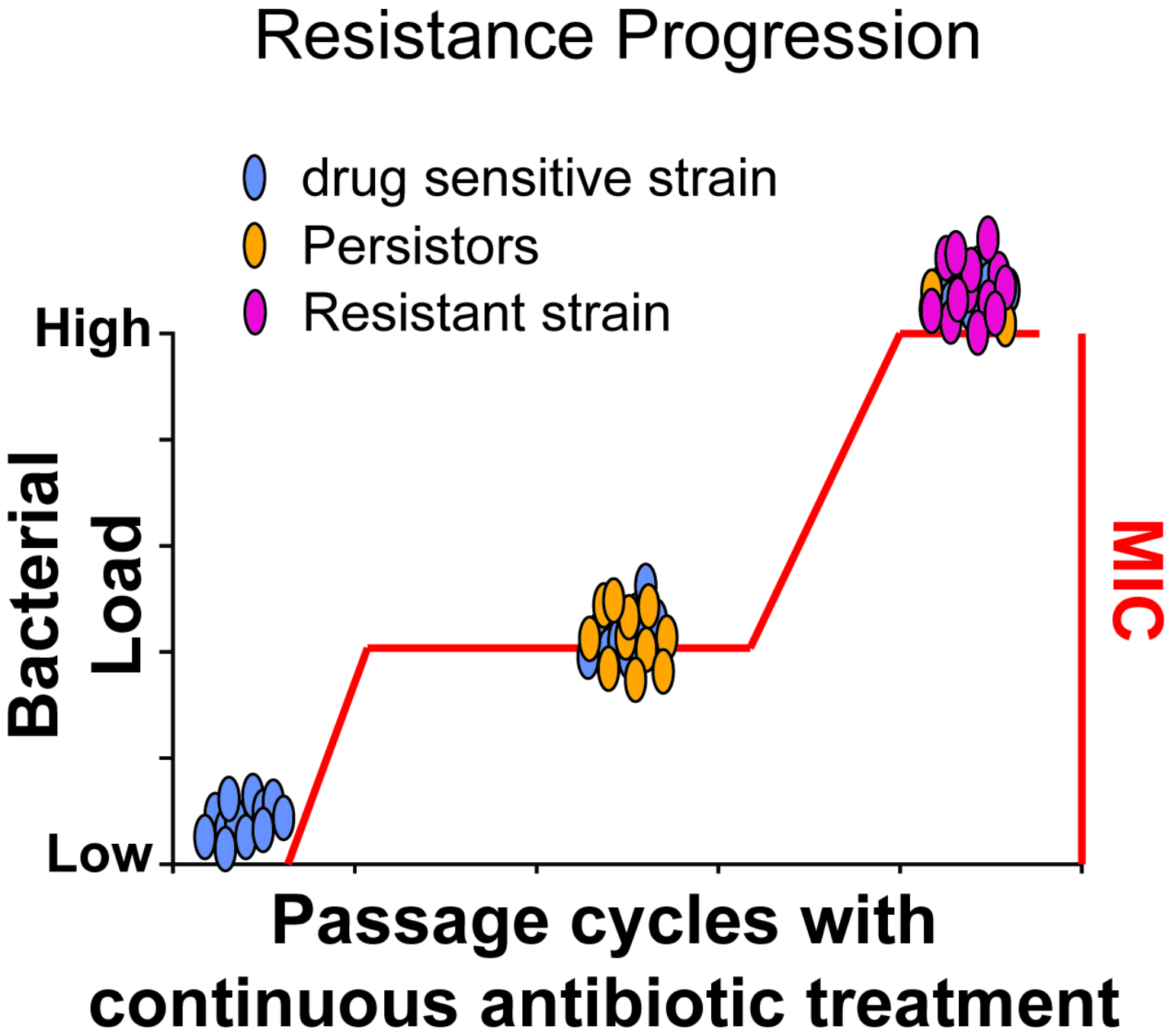
Resistance Progression
drug sensitive strain
Persistors
Resistant strain
High
Low
Bacterial Load
MIC
Passage cycles with continuous antibiotic treatment

Table S1. Strains used in this study.

Clone name	Description	Accession	Cipro MIC	reference	Relevant alleles
DH5α	*E. coli:* F⁻ *endA1 glnV44 thi-1 recA1 relA1 gyrA96 deoR nupG purB20* φ80d*lacZ*ΔM15 Δ(*lacZYA-argF*)U169, hsdR17($_{rK}^{-}{}_{mK}^{+}$), λ^{-}	N/A	N/A	70	N/A
DH5α λ*pir*	DH5α encoding π protein	N/A	N/A	71	N/A
WT/AB17978	*A. baumannii* ATCC 17978	SRX9736139	0.5	72	N/A
Ab12	Single colonies selected without CIP from immunocompetent L1: 15 passages	SRX9736138	0.5	This study	*ispB* R49H; ΔCP012005
Ab11		SRX12722651	0.5	This study	*ispB* R49H; *acx60_02425* V138I
Ab21	Single colonies selected without CIP from immunocompetent L2: 15 passages	SRX9736117	0.5	This study	*ispB* R49H; soxF V374*fs*
Ab22		SRX9736106	0.5	This study	*adeS* F114L; ACX60_04790 S27fs
Ab31	Single colonies selected without CIP from immunocompetent L3: 15 passages	SRX9736104	0.5	This study	*alaA* H391fs
Ab33		SRX12722652	0.5	This study	MrcB 768delN
CIPP10 Ab11	Single colonies CIP 1 μg/mL selection from immunocompetent L1: 10 passages	SRX12722636	4	This study	*obg* Δ12bp; AdeL C312*; Mmg V193M; PntB P363S
CIPP10 Ab12		SRX12722647	2	This study	AdeL C312*; Mmg V193M; PntB P363S
CIPP10 Ab13		SRX12722621	2	This study	AdeL C312*; Mmg V193M; PntB P363S
CIPP10 Ab14		SRX12722622	2	This study	AdeL C312*; RsgA Q45*
CIPP10 Ab21	Single colonies CIP 1 μg/mL selection from immunocompetent L2: 10 passages	SRX12722623	1	This study	AdeL C312*
CIPP10 Ab22		SRX12722624	1	This study	AdeL C312*
CIPP10 Ab23		SRX12722625	1	This study	AdeL C312*; GyrA R241C
CIPP10 Ab24		SRX12722626	1	This study	AdeL C312*; $utcC_{intergenic}$

CIPP10 Ab31	Single colonies CIP 1 μg/mL selection from immunocompetent L3: 10 passages	SRX12722653	1	This study	AdeL C312*; ComL K197N; ΔCP012005
CIPP10 Ab32		SRX12722627	1	This study	AdeL C312*; ComL K197N
CIPP10 Ab33		SRX12722628	1	This study	AdeL C312*; ComL K197N
CIPP10 Ab34		SRX12722629	1	This study	AdeL C312*; ComL K197N
CIPP15 Ab21	Single colonies CIP 1 μg/mL selection from immunocompetent L2: 15 passages	SRX12722630	1	This study	RplN M7L
CIPP15 Ab22		SRX12722631	1	This study	AdeL C312*
CIPP15 Ab23		SRX12722632	1	This study	PrmA S217I; ACX60_07895 A43fs
CIPP15 Ab24		SRX12722633	1	This study	AdeL C312*
CIPP15 Ab25		SRX12722634	1	This study	AdeL C312*
CIPP15 Ab26		SRX12722635	1	This study	AdeL C312*
Cy11	Single colonies selected without CIP from neutrophil-depleted mice lineage 1: 15 passages	SRX9736134	4	This study	*gyrB* Q447H; *adeL* C312*
Cy12		SRX9736133	4	This study	*gyrB* Q447H; *adeL* C312*
Cy21	Single colonies selected without CIP from neutrophil-depleted mice lineage 2: 15 passages	SRX9736132	8	This study	*gyrA* A117E
Cy22		SRX9736131	8	This study	*gyrA* A117E
Cy31	Single colonies selected without CIP from neutrophil-depleted mice lineage 3: 15 passages	SRX9736130	4	This study	*acfR* V136D; *adeL* P131H; *lpxD* insA; *mfsA*(-9)
Cy32		SRX9736129	4	This study	*acfR* V136D; *adeL* P131H; *lpxD* insA; *mfsA*(-9)
CIPCy11	Single colonies selected with CIP 1 μg/mL from neutrophil-depleted mice lineage 1: 15 passages	SRX12722637	4	This study	*gyrB* Q447H; *adeL* C312*
CIPCy13		SRX12722638	4	This study	*gyrB* Q447H; *adeL* C312*

CIPCy21	Single colonies selected with CIP 1 μg/mL from neutrophil-depleted mice lineage 2: 15 passages	SRX12722639	4	This study	*acfR* V136D; *adeL* P131H; *lpxD* insA; *mfsA*(-9)
CIPCy22		SRX12722640	4	This study	*acfR* V136D; *adeL* P131H; *lpxD* insA; *mfsA*(-9)
CIPCy32	Single colonies selected with CIP 1 μg/mL from neutrophil-depleted mice lineage 3: 15 passages	SRX12722641	4	This study	*acfR* V136D; *adeL* P131H; *lpxD* insA; *mfsA*(-9)
CIPCy33		SRX12722642	4	This study	*acfR* V136D; *adeL* P131H; *lpxD* insA; *mfsA*(-9)
P9Cy2.1	Single colony selected from neutrophil-depleted mice lineage 2: 9 passages	SRX9736110	1	This study	*adeL* Y324*
P9Cy3.1	Single colony selected from neutrophil-depleted mice lineage 3: 9 passages	SRX9736109	1	This study	*adeL* ΔI335A336
WH_B3	AB17978 *gyrB* Q447H	SRX9736122	0.5	This study	*gyrB* Q447H
WH113	AB17978 *adeL* C312*	SRX9736121	1	This study	*adeL* C312*
WH114	AB17978 *lpxD* T118_A119insA	SRX9736120	0.25	This study	*lpxD* T118_A119insA
WH309	AB17978 *lpxD* E117K	SRX9736119	0.25	This study	*lpxD* E117K
WH115	AB17978 *acfR* V136D	SRX9736118	0.25	This study	*acfR* V136D
WH_mfsA_48	AB17978 *mfsA*(-9)	SRX9736116	0.75	This study	*mfsA*(-9) A->G
WH_mfsA_12	AB17978 *mfsA*(-19)	SRX9736115	0.75	This study	*mfsA*(-19) T->A
WH319	AB17978 *mfs*(-9) *adeL* P131H	SRX9736114	4	This study	*mfs*(-9); *adeL* P131H
WH316	AB17978 *mfs*(-19) *adeL* P131H	SRX9736113	2	This study	*mfs*(-19); *adeL* P131H
JH1	AB17978 *mfsA*(-19) *adeL* ΔI335A336	SRX9736112	3	This study	*mfsA*(-19); *adeL* ΔI335A336
WH124	AB17978 *lpxD* insA *acfR* V136D *adeL* P131H	SRX9736111	0.75	This study	*lpxD* insA; *acfR* V136D; *adeL* P131H
EHA8	AB17978 *adeL* ΔIA	SRX9736108	1	This study	*adeL* ΔI335A336
EHA15	AB17978 *adeL* P131H	SRX9736107	1	This study	*adeL* P131H
EHA123	AB17978 *adeL* ΔIA Δ*adeFGH*	SRX9736105	1	This study	*adeL* ΔI335A336; Δ*adeFGH*

2 **Table S2. Plasmids and primers used in this study.**

Plasmid	**Description**	**Reference**
pUC18	*oriColE1* MCS AmpR	68
pJB4648	R6K ori (E. coli), GentR	69,71
Primers	**Sequence**	
qRT_PCR primers		
16s_qRT_For	CAGCTCGTGTCGTGAGATGT	
16s_qRT_Rev	CGTAAGGGCCATGATGACTT	
adeG_qRT_For	tgctgaaacggttgcatctc	
adeG_qRT_Rev	acggttttgaaccaattgttgg	
adeB_qRT_For	tccggtacagcagagattac	
adeB_qRT_Rev	tgaagcctcaacctgtaaac	
adeJ_qRT_For	cttgaagaacgtgagtctgg	
adeJ_qRT_Rev	attgcaccaatgacaccaag	
15145_qRT_For	GGGCACATACGACGAACTGA	
15145_qRT_Rev	CAAGCGCCACATTTTGACCA	
15150_qRT_For	GTTTTCCGCCAACTCAGCAC	
15150_qRT_Rev	ATCGCCAACGCAAATAGGGA	
Mutant construct primers		
mfsA_For_BamHI	CGCGGATCCTGTTTAACCTGCAACTGCGC	
mfsA_Rev_SalI	ACGCGTCGACCAAGCCTTCAGGACCGACTT	
AdeL_For_BamHI	CGCGGATCCGAAATGTACGGCAATGAG	
AdeL_Rev_Long_SalI	ACGCGTCGACCGAATCACCTTCCAATCCTT	
AraC_For_NotI	ATAAGAATGCGGCCGCCCGTGTTGAGCTTCTTGTTT	
AraC_Rev_XmaI	TCCCCCCGGGCGTCTACTCCTGCCGCAA	
LpxD_For_BamHI	CGCGGATCCCTGGTTATGGGGTAATTGATC	
LpxD_Rev_SalI	ACGCGTCGACGGTTTTGGCGTTTCATTGT	
GyrB_For_BamHI	CGCGGATCCGCCTCTCAAACAGAACAAACC	

GyrB_Rev_SalI	ACGCGTCGACGTGGTTCAACATCATCGCCC

3

Table S3. *in vitro* growth rates of LpxD mutants compared to AB17978.

Time (hr)		AB17978				AB17978::LpxD T118_A119insA				AB17978::LpxD E117K			
Optical density at 600nm	0	0.003	0.004	0.005	0.004	0.003	0.004	0.004	0.004	0.004	0.004	0.004	0.004
	1	0.015	0.015	0.015	0.013	0.009	0.011	0.011	0.011	0.014	0.014	0.014	0.013
	2	0.144	0.138	0.143	0.131	0.054	0.059	0.064	0.067	0.124	0.132	0.129	0.12
	3	1.085	1.01	1.01	0.97	0.335	0.37	0.395	0.43	0.935	0.975	0.985	0.825
	4	2.47	2.68	2.445	2.38	1.16	1.27	1.355	1.39	2.36	2.475	2.475	2.27
	5	3.79	3.82	3.78	3.8	2.81	2.98	2.92	3.12	3.64	3.79	3.64	3.76
	6	4.26	4.23	4.3	4.29	3.56	3.52	3.57	3.81	4.41	4.31	4.33	4.12
	7	4.5	4.59	4.67	4.64	3.95	3.97	3.99	4.09	4.69	4.4	4.47	4.55
	8	4.3	4.29	4.58	4.64	4.34	4.36	4.23	4.28	4.44	4.44	4.49	4.32
Doubling time(min)		**17.325**	**17.479**	**17.667**	**17.258**	**21.579**	**21.904**	**21.563**	**21.165**	**17.927**	**17.511**	**17.546**	**18.005**
R^2		**0.999**	**1**	**0.995**	**0.996**	**1**	**1**	**1**	**0.999**	**0.999**	**0.999**	**0.999**	**0.998**

Table S4. *in vitro* growth rates of the isolates acquired from the *in vivo* passaging experiments.

Time (hr)		AB17978			AB17978::*adeL* ΔIA			Cy11			Cy21			Cy31		
Optical density at 600nm	0	0.001	0.001	0.001	0.001	0.001	0.001	0.001	0.001	0.001	0.001	0.001	0.001	0.001	0.001	0.001
	1	0.004	0.002	0.004	0.003	0.003	0.003	0.003	0.003	0.003	0.003	0.003	0.003	0.003	0.004	0.003
	2	0.02	0.021	0.025	0.013	0.015	0.014	0.012	0.011	0.011	0.014	0.012	0.013	0.017	0.015	0.015
	3	0.106	0.182	0.201	0.074	0.077	0.055	0.034	0.042	0.03	0.059	0.042	0.049	0.109	0.052	0.094
	4	0.566	0.712	0.747	0.417	0.416	0.284	0.111	0.235	0.084	0.33	0.22	0.222	0.532	0.272	0.488
	5	1.6	1.65	1.8	1.22	1.2	0.99	0.65	0.9	0.51	1.02	0.93	1.95	1.23	1.03	1.24
	6	2.03	2.04	2.12	1.44	1.38	1.3	1.06	1.23	0.94	1.35	1.23	1.22	1.55	1.36	1.55
	7	2.3	2.29	2.5	1.69	1.76	1.63	1.38	1.54	1.1	1.57	1.5	1.39	1.88	1.74	1.78
	8	2.56	2.55	2.7	1.85	1.83	1.89	1.51	1.73	1.37	1.78	1.61	1.57	2.01	1.91	2
Doubling time(min)		**21.463**	**17.147**	**19.693**	**20.828**	**21.57**	**23.843**	**27.629**	**23.331**	**28.985**	**22.828**	**23.691**	**21.038**	**20.606**	**24.404**	**20.682**
R^2		**0.993**	**0.986**	**0.999**	**0.996**	**0.997**	**0.996**	**0.987**	**0.992**	**0.984**	**0.995**	**0.99**	**0.975**	**0.999**	**0.984**	**0.998**

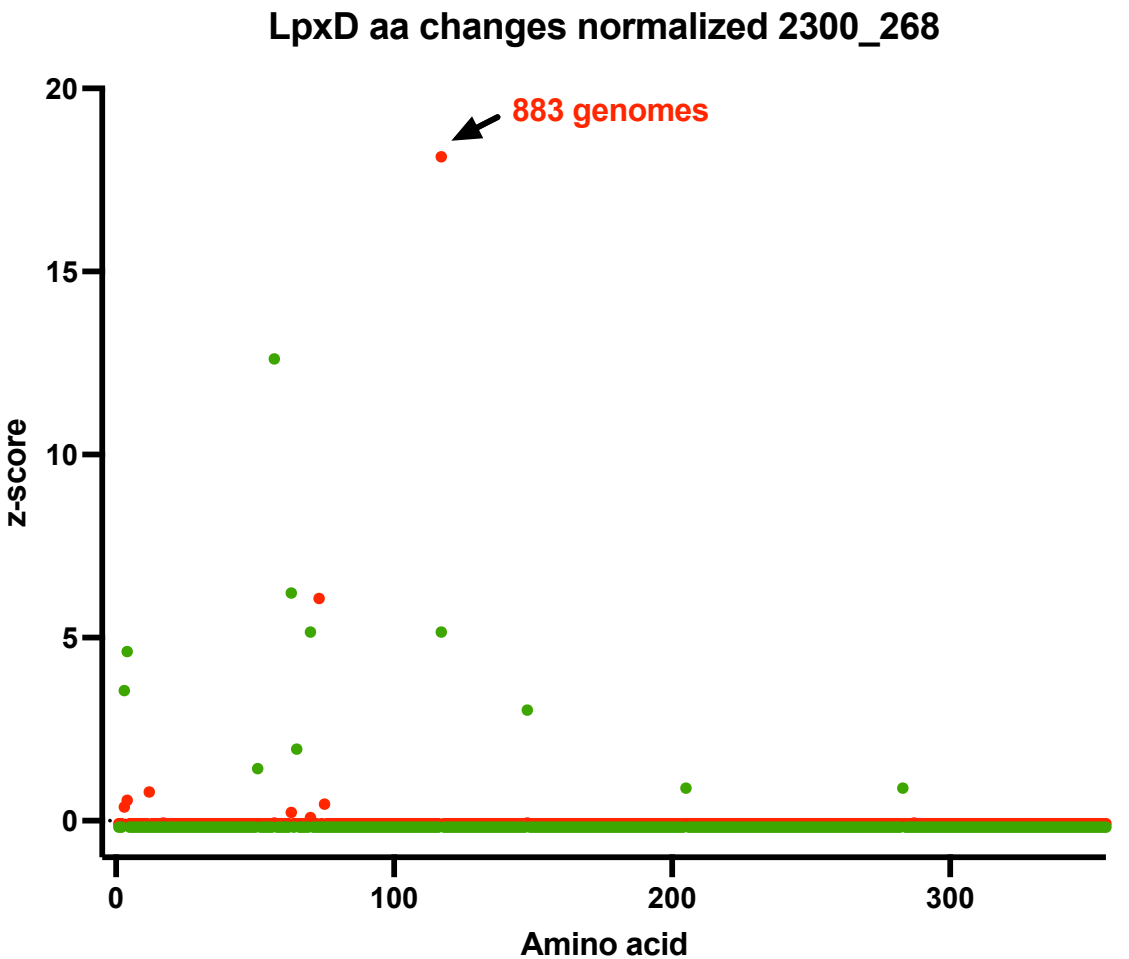
LpxD aa changes normalized 2300_268
883 genomes
z-score
20
15
10
5
0
0
100
200
300
Amino acid

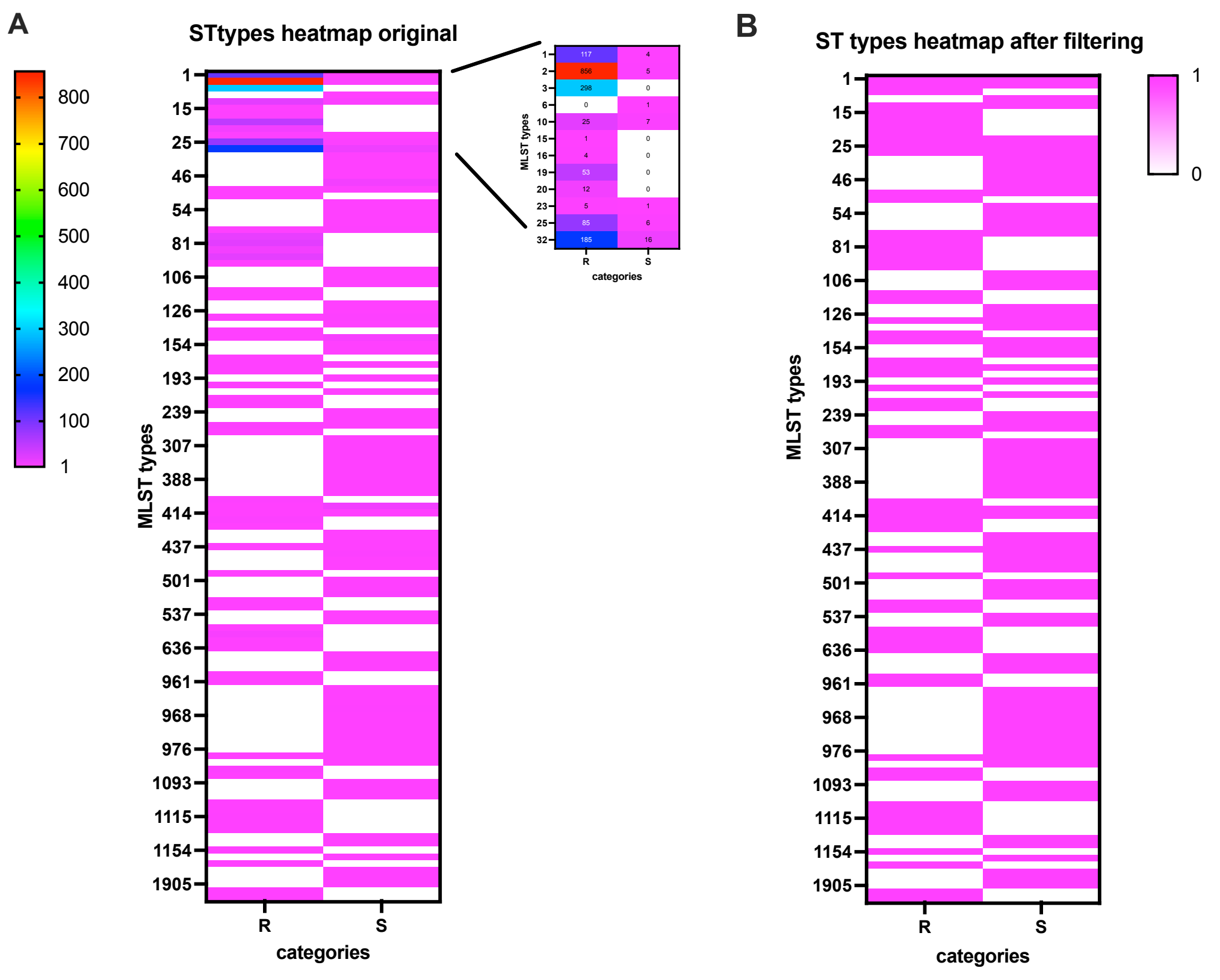
A
STtypes heatmap original
800
700
600
500
400
300
200
100
1
MLST types
1
15
25
46
54
81
106
126
154
193
239
307
388
414
437
501
537
636
961
968
976
1093
1115
1154
1905
R
S
categories
MLST types
1 117 4
2 856 5
3 298 0
6 0 1
10 25 7
15 1 0
16 4 0
19 53 0
20 12 0
23 5 1
25 85 6
32 185 16
R
S
categories
B
ST types heatmap after filtering
1
0
MLST types
1
15
25
46
54
81
106
126
154
193
239
307
388
414
437
501
537
636
961
968
976
1093
1115
1154
1905
R
S
categories

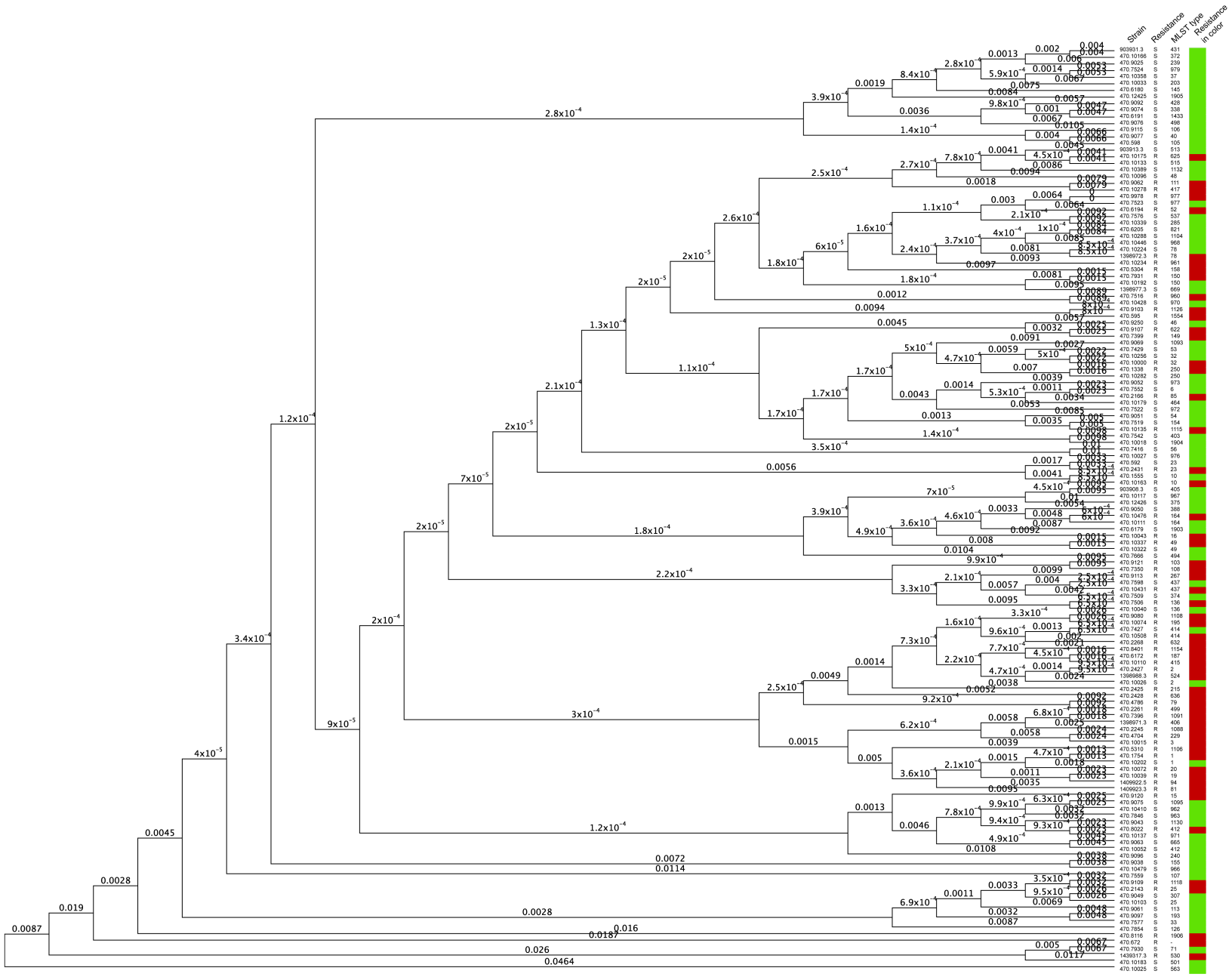
Strain
Resistance
MLST type
Resistance in color

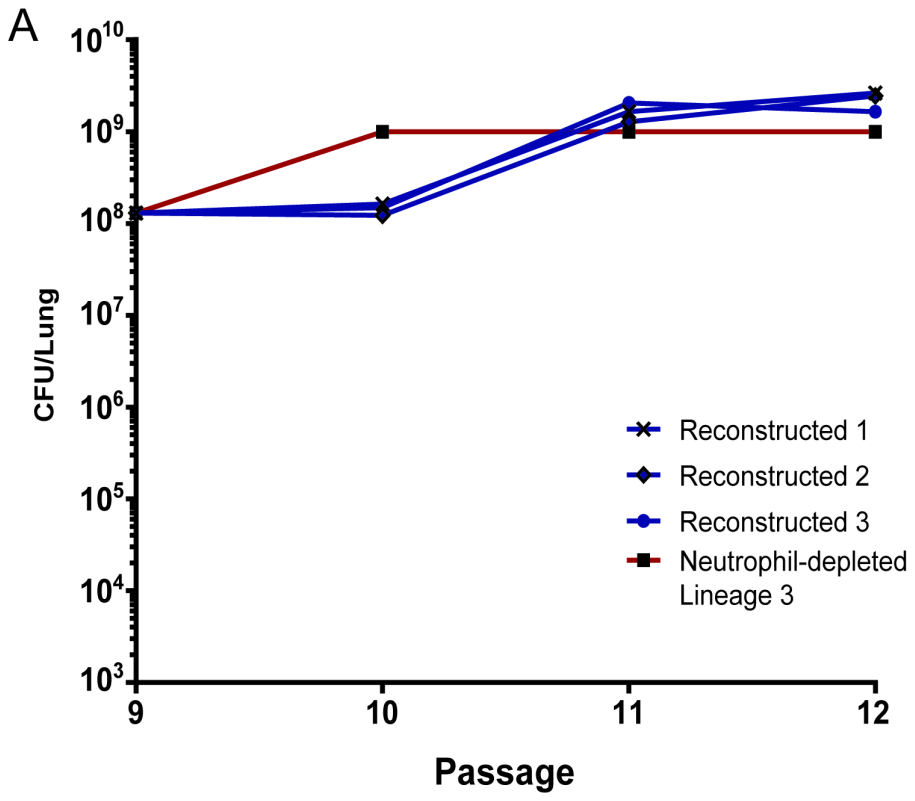
A
CFU/Lung
10^{10}
10^{9}
10^{8}
10^{7}
10^{6}
10^{5}
10^{4}
10^{3}
9
10
11
12
Passage
Reconstructed 1
Reconstructed 2
Reconstructed 3
Neutrophil-depleted Lineage 3

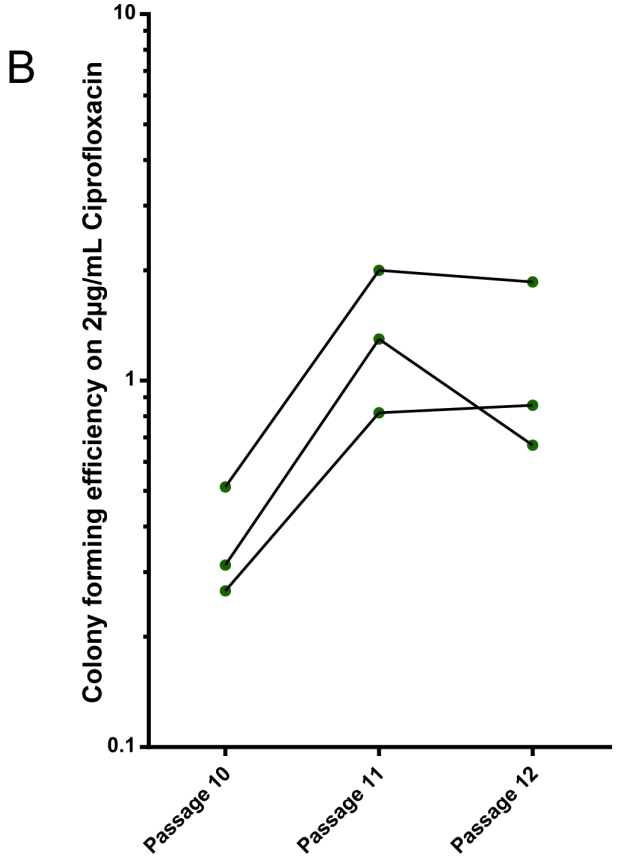
B
Colony forming efficiency on 2µg/mL Ciprofloxacin
10
1
0.1
Passage 10
Passage 11
Passage 12